1 **TITLE: RTP801 IS A KEY MODULATOR FOR MOTOR LEARNING**

2

3 Abbreviated title: **RTP801 in motor learning**

4

5 **AUTHORS:** Pérez-Sisqués L[1,2#], Martín-Flores N[1,2#a], Masana M[1,2,3,4], Solana J[1,2], Llobet A[1],

6 Romaní-Aumedes J[1,2], Canal M[1,2$], Campoy G[1,2], García-García E.[1,2,3,4], Sánchez-

7 Fernández N[1], Fernández-García S[1,2,3,4], Gilbert JP[5], Rodríguez MJ[1,2,3,4], Man H-Y[5],

8 Feinstein E[6], Williamson D[7], Soto D[1,2,3], Gasull X[1,2,3], Alberch J[1,2,3,4] and Malagelada C[1,2]*

9

10 [1] Department of Biomedicine, Faculty of Medicine, University of Barcelona, Catalonia, Spain
11 [2] Institut de Neurociències, University of Barcelona, 08036 Catalonia, Spain
12 [3] IDIBAPS- Institut d'Investigacions BiomèdiquesAugust Pi i Sunyer, Barcelona, 08036
13 Catalonia, Spain
14 [4] Centro de Investigación Biomédica en Red sobre Enfermedades Neurodegenerativas
15 (CIBERNED), Barcelona, 08036 Catalonia, Spain
16 [5] Department of Biology, Pharmacology and Experimental Therapeutics, Boston University,
17 Boston, MA, 02215USA
18 [6] Quark Pharmaceuticals, Fremont, CA, 94555 USA
19 [7] Kinesiology Program, School of Behavioral Sciences and Education, Penn State
20 Harrisburg, Middletown, PA,17057 USA
21 [a] Current affiliation: Department of Cell and Developmental Biology, University College
22 London, London, WC1E 6BT, UK
23 [$] Current affiliation: HIPRA Headquarters, Amer (Girona) 17170, Catalonia, Spain
24 [#] These authors contributed equally to this work.
25
26 *Correspondence: Cristina Malagelada, PhD. Unit of Biochemistry, Department de
27 Biomedicine, Faculty of Medicine. Address: Casanova 143, north wing 3rd floor; Universitat
28 de Barcelona, Barcelona 08036 Catalonia, (Spain) +34-934021919
29 E-mail: cristina.malagelada@ub.edu
30 ORCID: 0000-0001-7185-436X
31

32

33 **KEY WORDS:** GluA1 / motor learning / mTOR / Plasticity / RTP801 /

34

35

36

37

38

ABSTRACT:

RTP801/REDD1 is a stress-regulated protein whose upregulation is necessary and sufficient to trigger neuronal death in *in vitro* and *in vivo* models of Parkinson's and Huntington's diseases and is up regulated in compromised neurons in human postmortem brains of both neurodegenerative disorders. Indeed, in both Parkinson's and Huntington's disease mouse models, RTP801 knockdown alleviates motor-learning deficits.

Here, we investigated the physiological role of RTP801 in neuronal plasticity. RTP801 is found in rat, mouse and human synapses. The absence of RTP801 enhanced excitatory synaptic transmission in both neuronal cultures and brain slices from RTP801 knock-out (KO) mice. Indeed, RTP801 KO mice showed improved motor learning, which correlated with lower spine density but increased basal filopodia and mushroom spines in the motor cortex layer V. This paralleled with higher levels of synaptosomal GluA1 and TrkB receptors in homogenates derived from KO mice motor cortex, proteins that are associated with synaptic strengthening. Altogether, these results indicate that RTP801 has an important role modulating neuronal plasticity in motor learning.

INTRODUCTION:

Synaptic plasticity is the ability to fine tune neuronal connectivity and dynamics upon demand, for example in situations in which individuals have to adjust movements in challenging environments. This process is known as motor learning and involves the acquisition of a novel motor skill that, once learned, persists after training period ends (Peters *et al*, 2017; Sanes & Donoghue, 2000; Xu *et al*, 2009).

The central hub for motor learning is the motor cortex, an interconnected structure with other brain regions such as the striatum, the thalamus, brainstem or the spinal cord (reviewed in

67   (Shepherd, 2013; Shepherd & Huganir, 2007)). The complex process of acquiring new motor

68   skills induces synaptic plasticity in the motor cortex and requires dendritic spine formation,

69   consolidation and/or elimination, all leading to a necessary synaptic remodeling and

70   strengthening (Peters *et al*, 2017; Sanes & Donoghue, 2000; Fu *et al*, 2012; Xu *et al*, 2009).

71   Pyramidal neurons from the motor cortex and striatal medium spiny neurons (MSNs)

72   predominantly undergo plastic changes along motor learning (Costa *et al*, 2004; Tjia *et al*,

73   2017). Regarding the motor cortex, projection pyramidal neurons from Layer V (LV) are the

74   main excitatory input to the striatum involved in the corticostriatal pathway (Costa *et al*,

75   2004; Shepherd & Huganir, 2007; Hintiryan *et al*, 2016; Anderson *et al*, 2010). These plastic

76   changes leading to motor learning involve, at least, increased levels of α-amino-3-hydroxy-5-

77   methyl-4-isoxazolepropionic acid receptors (AMPAR) at dendritic spines (Kida *et al*, 2016;

78   Roth *et al*, 2020) . However, the mechanisms by which these events are regulated are not

79   yet clearly elucidated.

80

81   In many neurodegenerative diseases, along with neurological and psychiatric symptoms,

82   motor dysfunction is a hallmark of disease progression. Among these disorders, we find

83   Parkinson's disease (PD), Huntington's disease (HD), or amyotrophic lateral sclerosis,

84   (Shepherd, 2013). Motor dysfunction is due, in part, to an impairment in the synaptic

85   plasticity of the circuitries that control movement by interconnecting motor cortex and basal

86   ganglia and the thalamus, and also the cerebellum (Guo *et al*, 2015; Xu *et al*, 2017;

87   Calabresi *et al*, 2007, 2000).

88

89   RTP801/REDD1, coded by the *DDIT4* gene, is a stress-regulated protein that is sufficient

90   and necessary to induce neuron death (Shoshani *et al*, 2002; Malagelada *et al*, 2006). It is

91   elevated in cellular and animal models of PD in response to dopaminergic neurotoxins

92   (Malagelada *et al*, 2006; Ryu *et al*, 2005) and is highly up regulated in neuromelanin positive

93   neurons in the substantia nigra pars compacta (SNpc) of both sporadic (Malagelada *et al*,

94   2006) and parkin mutant PD patients (Romani-Aumedes *et al*, 2014). RTP801 induces

95   neuron death by a sequential inactivation of mTOR and the survival kinase Akt (Malagelada

96   *et al*, 2008) via the tuberous sclerosis complex 1/2 (TSC1/2). Regarding HD, RTP801 levels

97   are highly increased in HD human brains, in differentiated neurons derived from induced

98   pluripotent stem cells (iPSC) from HD patients (Martín-Flores *et al*, 2016) and in striatal

99   synapses from HD mouse models (Martín-Flores *et al*, 2020). Besides, in neuronal models

100   of the disease, RTP801 mediates mutant huntingtin (mhtt)-induced toxicity (Martin-Flores *et*

101   *al*, 2015). Importantly, RTP801 contributes to motor-learning dysfunction in HD since

102   RTP801 knockdown prevents from the appearance of motor learning deficits in the R6/1

103   model of the disease (Martín-Flores *et al*, 2020). This suggests that synaptic RTP801

104   deregulation is a common hallmark in neurodegeneration. Indeed, RTP801 coding gene

105   *DDIT4* was recently described as one of the top three common deregulated transcripts in

106   *postmortem* brain samples from PD and HD patients (Labadorf *et al*, 2018). Furthermore,

107   RTP801 is sufficient to cause neuronal atrophy and depressive-like behavior (Ota *et al*,

108   2014) and it has a regulatory role in cortical development, neuronal differentiation

109   (Malagelada *et al*, 2011) and peripheral nervous system myelination (Noseda *et al*, 2013).

110   However, its physiological role in synaptic plasticity has not been resolved yet. For this

111   reason, here we investigated the potential synaptic function of RTP801 in the corticostriatal

112   pathway. By using cellular and murine models and *postmortem* human brains and

113   performing behavioral, histological, electrophysiological and biochemical analysis, our

114   results describe the implication of RTP801 in motor learning plasticity.

115

116

117   **RESULTS:**

118

119   **RTP801 is localized in the synapses of murine and human samples and modulates**

120   **synaptic transmission *in vitro***

121   We first explored whether RTP801 was localized in synapses and whether it was involved in

122   synaptic function, connectivity and transmission. Hence, we first isolated cortical and striatal

4

123   crude synaptosomes from adult *postmortem* human brain, adult rat and mouse brains and

124   from cultured rat cortical neurons. In all samples we observed the presence of RTP801 or its

125   enrichment in crude isolated synaptic terminals in comparison to the initial homogenates

126   (**Fig 1 A**), corroborating our own previous results (Martín-Flores *et al*, 2020). Interestingly, in

127   cultured cortical neurons, we observed that RTP801 was expressed in the soma, dendrites

128   and dendritic spines (**Fig 1 B**).

129   We next investigated whether RTP801 depletion affected spine density and synaptic

130   transmission. For this, we knocked down the expression of RTP801 in cortical primary

131   cultures at 14DIV, using lentivirus expressing a specific shRNA for RTP801 or scramble

132   shRNA as control. We observed that RTP801 silencing induced a significant decrease in

133   spine density relative to the scramble shRNA transduced neurons (**Fig 1 C**). We next

134   analyzed whether RTP801 expression abrogation affected synapse function by evaluating

135   the frequency and the amplitude of mEPSCs of cortical cultures derived from WT and

136   RTP801 KO mice. Interestingly, in the complete absence of RTP801 expression using

137   cultured cortical neurons from RTP801 KO mice, we observed that both the amplitude (**Fig 1**

138   **D1, D2 & D.3**) and frequency (**Fig 1 D1. D2 & D.4**) of mEPSCs were higher than the ones

139   registered in WT cortical sister cultures.

140   We corroborated our *in vitro* results using cultured hippocampal neurons, a well

141   characterized plasticity model. In line with previous results, we found that RTP801

142   colocalized with PSD-95, an excitatory postsynaptic scaffold protein, but not with the

143   presynaptic marker SV2A, indicating that RTP801 is localized in the postsynaptic

144   compartment (**Fig EV1 A-B**). Moreover, ectopic RTP801 expression attenuated the

145   amplitude of mEPSCs without affecting the frequency, along with a decrease of PSD-95 and

146   AMPAR receptor subunit GluA1 puncta intensity (**Fig EV1 C-E**).

147

148   **Synaptic and behavioral characterization of RTP801 KO mice brains**

149   Previous data pointed out that the total abrogation of RTP801 expression did not influence

150   significantly either the brain structure or the basal behavior of the RTP801 KO mice in

151   comparison to WT animals (Brafman *et al*, 2004; Ota *et al*, 2014). However, we previously

152   demonstrated that RTP801 regulated the timing of cortical neurogenesis and neuron

153   differentiation/migration (Malagelada *et al*, 2011) using *in utero* electroporation techniques.

154   For this reason, to validate the use of the RTP801 KO mouse to study its putative synaptic

155   role, we characterized its brain morphology in comparison to WT animals. We first confirmed

156   the lack of RTP801 expression in the KO animals in motor cortex homogenates (**Fig 2 A**).

157   Macroscopically, although there were no differences in the mice body weight between

158   genotypes (**Fig 2 B**), we observed that KO animals presented a decreased brain weight (**Fig**

159   **2 C**). However, internal structural organization did not present major alterations either in

160   cortical layers, hippocampus or even in the striatum, as judged by Nissl staining (**Fig 2 D**).

161   Primary motor cortex (M1) layer thickness did not differ either between genotypes (**Fig 2 E**)

162   but RTP801 KO mice showed an expected decreased cell density in the M1 LV (**Fig 2 F**).

163

164   We next investigated whether cortical spine density was affected in the adult brain of

165   RTP801 KO mice using Golgi-Cox staining. Analyses were performed in the M1 layer V

166   pyramidal neurons, the main excitatory and direct projection to the ipsi- and contralateral

167   striatum in the corticostriatal pathway (Shepherd, 2013; Hintiryan *et al*, 2016; Anderson *et al*,

168   2010; Xu *et al*, 2009). As previously seen by knocking down RTP801 in cortical cultured

169   neurons (see **Fig 1 C**), we observed a reduction in the density of spines in LV neurons in

170   naive RTP801 KO mice compared to WT animals (**Fig 2 G**).

171

172   Next, we assessed whether RTP801 modulate synaptic transmission in cortical brain slices

173   from naïve WT and KO animals. We thus measured neuronal spike rate and bursting in M1

174   LV using multielectrode array (MEA) (**Fig 2 H**). We found an increased spike rate in the LV

175   of KO animals when compared with WT (**Fig 2 I.1**), with no differences between male and

176   female animals (**Fig EV2 A**). Analysis of spike-train patterns showed a higher burst rate and

177   proportion of spikes included in bursts in KO primary motor cortex slices when compared

178   with WT (**Figure 2 I.2-I.3**). We found no other differences in the burst parameters analyzed

179 (**Fig EV2 B-D**). These results support the hypothesis that neuronal excitability is increased in

180 LV motor cortex in KO mice as an attempt to compensate the decreased number of synaptic

181 spines.

182

183 To study whether synaptic structural and functional changes in RTP801 KO mice correlated

184 with behavioral alterations, we next investigated whether the lack of RTP801 affected

185 coordination, locomotion and motor learning. We first tested WT and KO mice for hindlimb

186 clasping, a marker of disease progression in a number of mouse models of

187 neurodegeneration, including HD (Mangiarini *et al*, 1996; Chou *et al*, 2008). We observed

188 that RTP801 KO male mice displayed a clasping phenotype, not present in male WT mice.

189 The tendency in females was similar but not significant (**Fig EV3 A**). We next explored

190 whether gait, as a measure of coordination and muscle function, was affected in RTP801 KO

191 mice. These animals showed a decrease in the length of the stride, stance, sway and the

192 overlap (**Fig 3 A-B** and **Fig EV3 B**), suggesting gait impairment in the KO animals. We next

193 examined whether general locomotor activity was altered using the Open Field test. Despite

194 gait impairment, we did not find any differences in the total distance travelled in the RTP801

195 KO mice relative to WT (**Fig 3 C**). We did not find differences in the distance travelled in the

196 center or the time spent in the center, suggesting that RTP801 KO mice do not exhibit

197 anxiety-like behavior. Regarding other general exploratory and stereotypic behavior, we did

198 not find any differences in grooming or wall and vertical rearing, either (**Fig EV3 C**).

199 To evaluate motor skill learning, we trained the WT and RTP801 KO animals in the

200 accelerating rotarod. Both female and male KO mice showed the same trend to improve

201 motor learning in this behavioral paradigm (**Fig EV3 D**). Together, RTP801 KO mice

202 significantly improved performance in this task compared to WT animals (Genotype effect, **

203 *P*=0.0058) (**Fig 3 D**). This result indicates that RTP801 is involved in motor learning

204 acquisition.

205

206 **RTP801 modulates spine density and structure in the primary motor cortex of trained**

207 **animals**

208 We next investigated whether the improvement in motor learning in the RTP801 KO mice

209 affected differentially spine density and structure. Hence, since motor learning plasticity

210 involves projections from the motor cortex to the dorsal striatum, we explored spine density

211 and morphology in pyramidal neurons from the M1 LV and in medium spiny neurons (MSNs)

212 from the dorsal striatum, one week after finishing the accelerating rotarod test (**Fig 4 A**).

213 Similar to non-trained naïve RTP801 KO mice, trained RTP801 KO mice showed a decrease

214 in the density of spines in LV pyramidal neurons (**Fig 4 B**), specifically in their basal

215 dendrites. Interestingly, spine density of either cortical LV apical dendrites or dendrites in

216 striatal MSNs did not change (**Fig 4 C-D**).

217

218 Based on these results, we investigated differences in spine morphology in the M1 LV

219 pyramidal neurons that could explain the increased motor learning in the KO mice. Indeed,

220 RTP801 KO animals displayed more filopodia but less branched spines (**Fig 5 A** and **Fig**

221 **EV4**). In line with this, when related with the total number of headed spines, we observed a

222 higher percentage of mushroom spines in the basal dendrites of KO animals (**Fig 5 B.1,**

223 **C.1**). Moreover, their head area was also increased. On the contrary, no differences were

224 found in either the percentage or head area of thin spines (**Fig 5 C.1, C.2**).

225 We next asked whether this evidence in LV pyramidal neurons based on Golgi-Cox staining

226 could be supported ultra-structurally by Transmission Electron Microscopy (TEM).

227 Interestingly, we observed that KO mice synapses had bigger postsynaptic area (around

228 10%) (**Fig 6 A**) along with a wider PSD area, length and thickness (around 5%, each) (**Fig 6**

229 **B**). Interestingly KO mice exhibited a higher percentage of contacts containing mitochondria,

230 mostly at the presynaptic compartment although the postsynaptic compartment showed a

231 similar tendency (**Fig 6 C**). We did not find significant differences in the percentage of

232 presynapses with more than one post-synapse, postsynapses with more than one

233 presynapse or postsynapses with spine apparatus (**Fig EV5 a-c**). Altogether, these results

234 support the idea that although the KO mice have a decreased number of spines in the motor

235 cortex LV, they displayed a more efficient synaptic structure, leading to an improvement of

236 motor learning skills.

237

238 **The lack of RTP801 elevates GluA1 AMPAR post-synaptically**

239 In line with the reduction in spine density in neurons from motor cortex LV in the RTP801 KO

240 mice (**Fig 4B**), biochemical analysis of KO motor cortex crude synaptic fractions confirmed a

241 decrease in PSD-95 (**Fig 7 A**) but an specific enrichment of synaptic GluA1 (**Fig 7 B**), a

242 crucial AMPAR subunit that has been described to be a key mediator in the acquisition of

243 new motor skills (Kida *et al*, 2016; Roth *et al*, 2020). On the other hand, GluA2 AMPAR

244 subunit, the prototypical auxiliary subunit of AMPARs stargazin or the N-methyl-D-

245 aspartate receptor (NMDAR) subunit GluN2B did not change in KO mice in comparison to

246 WT (**Fig 7 B-C**). Interestingly, we observed that levels of TrkB were also elevated in total

247 homogenates in the RTP801 KO motor cortex (**Fig 7 D**), supporting the idea of a synaptic

248 strengthening. By immunostaining WT and KO sections against PSD95 and GluA1

249 postsynaptic markers, we confirmed these initial biochemical observations specifically in M1

250 layer V. Indeed, the number of PSD-95 and GluA1 puncta diminished in the KO animals (**Fig

251 7E, H**) although the area and the intensity of the GluA1 dots were increased (**Fig 7 F-G**).

252 Area and intensity of PSD-95 positive dots showed a non-significant increased tendency, as

253 well (**Fig 7 F-G**). Altogether, these results suggest a novel synaptic role for RTP801

254 modulating synaptic strength and motor learning in the motor cortex (**Fig 8**).

255

256 **DISCUSSION**

257 Here, we show a novel role for RTP801 in the modulation of synaptic plasticity in motor

258 learning. The lack of RTP801 in mice resulted in decreased spine density and enhanced

259 synaptic transmission in the primary motor cortex together with a better performance in the

260 accelerating rotarod but altered gait and clasping. This improvement in motor learning skills

9

261 was associated with alterations in dendritic spine structure. Cortical neurons in the motor

262 cortex M1 layer V showed higher number of filopodia- and a mushroom-like morphology and

263 TEM analyses revealed increased postsynaptic size in neurons from LV. In line with that,

264 trained RTP801 KO mice showed higher levels of synaptic AMPAR subunit GluA1 and a

265 general increase in TrkB levels.

266

267 Since the only evidences that RTP801 could modulate synaptic plasticity were found in

268 pathological conditions, here we studied for the first time the putative role of RTP801 in a

269 physiological context. In a context of depressive disorders, RTP801 KO mice were found

270 resilient to stress-induced synaptic loss in the PFC (Ota *et al*, 2014; Kabir *et al*, 2017).

271 Moreover, RTP801 downregulation alleviated stress-induced neurodegeneration in a mouse

272 model of genetic PD (Zhang *et al*, 2018). More recently, our group described that synaptic

273 RTP801 mediated motor-learning dysfunction in the R6/1 mouse model of HD (Martín-Flores

274 *et al*, 2020). However, its potential physiological synaptic role has never been investigated in

275 depth.

276

277 Hence, we initially confirmed that RTP801 was present in the synapses from a wide range of

278 human and murine samples, as we previously described in HD murine models and HD

279 human postmortem samples (Martín-Flores *et al*, 2020). Interestingly, RTP801 was highly

280 enriched in human and rat crude synaptosomes but not that elevated in synaptic WT mice

281 samples. In line with that, in cortical cultures RTP801 was localized mostly post-sinaptically.

282 Interestingly, we found that spine density decreased in cortical cultures when RTP801

283 expression was transiently downregulated and that was translated with an increase in the

284 amplitude and frequency of mEPSCs in KO cortical cultures. An opposite effect was found

285 when ectopic RTP801 was expressed in hippocampal primary cultures.

286 Previous studies pointed out that RTP801 KO mice had normal brains and similar behavior

287 to WT animals (Brafman *et al,* 2004; Ota *et al*, 2014). However, no thorough behavioral,

288 biochemical and histological studies were performed in these animals. Macroscopically, we

289   found that the KO mice brain weight less than WT brains, independently of the total body

290   size, and it was likely due to a decrease in the cell density of M1 LV. Noteworthy, this

291   difference can be explained by the developmental role of RTP801, which regulates both

292   neurogenesis   by   regulating   neuroprogenitors'   proliferation   rate   and   neuronal

293   migration/differentiation in the cortex (Malagelada *et al*, 2011).

294

295   *In vivo*, the lack of RTP801 reduced spine density in the M1 layer V in the KO mice vs. WT.

296   We observed a similar result when we transiently downregulated RTP801 in cultured cortical

297   neurons (**Fig 1C**). Interestingly, KO animals showed higher synaptic performance in KO

298   motor cortex (LV) slices *versus* WT. These results therefore suggest that the lack of RTP801

299   decreases spine density but enhances synaptic function.

300

301   To investigate the role of RTP801 in synaptic plasticity *in vivo* we performed several motor

302   behavioral tests and checked circuitries that control movement and motor learning. RTP801

303   KO mice showed gait impairment but no alterations in general locomotor activity. It is

304   noteworthy that gait abnormalities are more likely to be explained by cerebellar dysfunction

305   and more studies will be needed in the future. Despite gait alterations, the lack of RTP801

306   improved mouse motor learning skills. These results are in line with the work of Zhang et al

307   (2018) (Zhang *et al*, 2018), where the knockdown of RTP801 in the substantia nigra partially

308   rescued motor function in a mouse model of PD subjected to chronic-restraint stress. In

309   addition, we recently described that striatal RTP801 knock down in the R6/1 mouse model of

310   HD prevented from motor-learning deficits (Martín-Flores *et al*, 2020).

311

312   The most characterized circuitry involved in motor learning is the corticostriatal pathway.

313   Pyramidal neurons from the M1 along with striatal MSNs predominantly undergo synaptic

314   dynamics under motor learning (Tjia *et al*, 2017; Costa *et al*, 2004). Indeed, spine density in

315   the M1 LV neurons from the RTP801 KO mice, specifically in their basal dendrites, was

316   decreased. We did not observe any differences in spine density in the apical dendrites of the

317   same neurons or in the striatal MSNs from the KO mice. Related to the cortex, Ota and

318   colleagues (Ota *et al*, 2014) did not find spine density differences in the prefrontal cortex

319   (PFC) between WT and RTP801 KO mice in basal conditions. This fact, together with the

320   absence of differences in the striatum in our work, may point towards a region-specific role

321   of RTP801 in the normal (or physiological, non-stressed) mouse brain. Hence, RTP801

322   could be contributing to motor learning at the basal dendrites of LV pyramidal neurons.

323

324   This speculation was also supported by the observations of the synaptic morphology in the

325   motor cortex LV pyramidal neurons, where we observed a significant increase of filopodia

326   along with a decrease in branched spines in the KO animals. Although the physiological

327   meaning of branched spines is still in debate, filopodia have been proposed to be precursors

328   of spines, to develop an explorative role to increase the probability to form a synapse (Ziv &

329   Smith, 1996; Zuo *et al*, 2005). Thus, an increase in this type of spines could explain the

330   better performance of the KO mice in the accelerating rotarod. However, filopodia-related

331   plasticity must have a fine-tuned regulation, since a high remodeling rate might be

332   troublesome (reviewed in (Ozcan, 2017)). Indeed, among headed spines, we detected an

333   increase in the percentage and head area of mushroom-like spines from basal dendrites

334   between WT and KO animals. This fact correlates well with the change of spine morphology

335   and the function of the spines, and in the end, with an increase in synaptic strength of the

336   area (Arellano *et al*, 2007; Yuste *et al*, 2000).

337

338   We confirmed a more complex postsynaptic compartment by TEM. The lack of RTP801 led

339   to an increase in postsynaptic area in the synapses of the region of study, although no

340   differences were detected in the presynaptic compartment. Strikingly, greater postsynaptic

341   density size was detected in RTP801 KO animals in the same area. Interestingly, a positive

342   correlation between the amount of PSD and spine size (Arellano *et al*, 2007) and the former

343   with synaptic strength (Béïque & Andrade, 2003; Meyer *et al*, 2014) has been described.

344   Moreover, KO synaptic contacts present more mitochondria, whose presence at the synapse

345   has been related with a role in controlling plasticity processes (Todorova & Blokland, 2017;

346   Lee *et al*, 2018)). Our ultrastructural analyses, therefore, seem to indicate that, although the

347   lack of RTP801 causes a decrease in spine density, the remaining spines are able to

348   compensate this reduction at a structural level.

349

350   Interestingly, we observed a differential synaptic composition in the remaining spines in the

351   M1 LV from RTP801 KO mice versus WT animals. We observed decreased levels of

352   synaptic PSD-95 in crude synaptosomes that go in line with the decreased number of PSD-

353   95 positive puncta in M1 LV observed by immunohistochemistry, along with a specific

354   elevation of GluA1 AMPAR subunit at the synapses in M1 LV of KO mice. Calcium

355   impermeable AMPARs (GluA2-containing; CI-AMPARs) are the most prevalent type of

356   AMPAR in neurons (Lu *et al*, 2009) where they are responsible for postsynaptic currents and

357   the depolarization of the postsynaptic neuron. In contrast, GluA1 subunit confers calcium

358   permeability to the receptor. Calcium permeable AMPAR (CP-AMPARs) are mostly engaged

359   to synaptic regulation and intracellular signaling (reviewed in (Man, 2011). Therefore, the

360   improved performance observed in the KO mice could be explained at least in part with this

361   change in the AMPA receptors subunit composition. This could favor the presence of CP-

362   AMPARs with high calcium permeability and then, in consequence, signaling activation and

363   synaptic regulation. Interestingly, previous studies have demonstrated that motor learning

364   induces an increase in GluA1 levels in dendritic spines in the motor cortex. This increment in

365   GluA1 subunits are key modulators of synaptic plasticity induced by motor skill learning

366   (Roth *et al*, 2020). The mechanism by which RTP801 could mediate this specific AMPAR

367   subunits composition at the synapses to modulate motor learning has to be explored yet.

368   Ectopic RTP801 overexpression showed the opposite result, since it reduced GluA1 puncta

369   intensity in cultured hippocampal neurons. Remarkably, RTP801 silencing in R6/1 mice

370   induced an increase of total levels of GluA1 and TrkB neurotrophin receptor. Indeed, in

371   trained RTP801 KO mice we could also observe an increase in total levels of TrkB receptor.

372   This result is in line with other works describing that synaptic activity modulates both BDNF

373   levels and TrkB receptors amount and localization (Guo *et al*, 2014; Lauterborn *et al*, 2000).

374

375   In summary, our work indicates a novel synaptic function for RTP801 in motor learning by

376   modulating synaptic structure, composition and plasticity. This finding is important since

377   motor learning impairment is a key feature of neurodegenerative diseases such as PD and

378   HD. Altogether, our results point towards RTP801 downregulation as a promising

379   therapeutic strategy to ameliorate motor learning dysfunction in these diseases.

380

381   **MATERIALS AND METHODS**

382

383   **Animals**

384   Transgenic RTP801 knock out mouse strain was generated by Lexicon Inc. as described in

385   (Brafman *et al*, 2004). RTP801 knockout mice were obtained by homozygous pairing. Thus,

386   wild type mice were bred from the RTP801 KO founder strains to obtain a C57Bl6/129sv

387   background. RTP801 knock out and wild type mice were housed under controlled conditions

388   (22ºC, 40-60% humidity in a 12-hour light/dark cycle) with water and food available *ad*

389   *libitum*. All the animals analyzed in this study were 2 months-old adult mice.

390

391   For further biochemical analyses, Golgi staining and TEM, mice were euthanized by cervical

392   dislocation and tissue was dissected out. For immunohistochemistry, animals were

393   processed as described elsewhere (Creus-Muncunill *et al*, 2018). Briefly, animals were

394   anesthetized with 60mg/kg dolethal and intracardially perfused with 4% PFA. Coronal 25µm-

395   thick brain sections were obtained with a cryostat.

396

397   **Rat primary cultures**

398   Rat cortical and hippocampal primary cultures were obtained from embryonic day 18

399   Sprague-Dawley rats as previously described (Canal *et al*, 2016). Cells were either

400   transduced with lentiviral particles carrying a control shRNA or a specific shRNA against

401   RTP801 or transfected with lipofectamine 2000 (Thermo Fisher Scientific) with pCMS

402   vectors expressing eGFP (donated by Dr. Lloyd Greene, Columbia University) or eGFP-

403   fused RTP801 protein (Romaní-Aumedes *et al*, 2014). The sequences to downregulate or

404   overexpress RTP801 were previously described in (Malagelada *et al*, 2006).

405

Mouse primary cultures

407   Mouse primary cortical cultures were obtained from embryonic day 15 mice. Coverslips were

408   coated for 1h with 0.1 mg/ml poly-D-lysine (Merck) and then 3.5h with 0.018 mg/ml laminin

409   (Thermo Fisher Scientific). Briefly, cortices were dissected out and chemically digested with

410   41.66μM Trypsin for 10 minutes. Following mechanical digestion, cells were plated on

411   coverslips at a density of 25.000 cells/cm^2 and maintained in Neurobasal-A medium

412   supplemented with B27, GlutaMAX (all from Gibco), 33.3 mM Glucose and 1% penicillin-

413   streptomycin (Sigma) in a 5% CO_2 atmosphere and 37ºC.

414

Crude synaptosomal fractionation

416   Tissue (rat, mice or *postmortem* human brains) or cultured cells were homogenized in

417   Krebs-Ringer buffer (125mM NaCl, 1.2mM KCl, 22mM NaHCO3, 1mM NaH2PO4, 1.2mM

418   MgSO4, 1.2mM CaCl2, 10 mM Glucose, 0.32 M Sucrose; pH 7.4). For samples in Figure 7,

419   mice were sacrificed one week after behavioral testing. Initial lysate was first centrifuged at

420   1.000g for 10 minutes. Supernatant (homogenate) was centrifuged for 20 minutes at

421   16.000g to obtain the cytosolic fraction (supernatant) and the crude synaptosomal fraction

422   (pellet), that was resuspended in Krebs-Ringer buffer.

423

Western blotting

425   Samples were resolved in NuPAGE^{TM}Novex^{TM} polyacrylamide gels and proteins were

426   transferred to nitrocellulose membranes with the iBlot system (all from Thermo Fisher

427   Scientific). Indicated primary antibodies were incubated overnight at 4ºC diluted in Tris-

428 buffered saline containing 0.1% Tween-20 and 5% BSA. Secondary antibodies (Thermo

429 Fisher Scientific) were diluted in TBS-Tween with non-fat dry 5% milk (Bio-rad) for 1 hour.

430 Proteins were detected with Supersignal^{TM} West Pico Plus chemiluminiscent substrate

431 (Thermo Fisher Scientific) and images were acquired with ChemiDoc^{TM} (Bio-Rad). The

432 following antibodies were used: RTP801 (1:500, Proteintech), HRP-conjugated anti-beta

433 actin (1:100.000; Sigma), PSD-95 (1:1000; Thermo Fisher Scientific), SV2a and GFP

434 (1:1000; Santa Cruz Biotechnology), GluA1, GluA2, Stargazin (1:1000; Merck Millipore),

435 GluN2B (1:1000; Cell Signaling Technology) and TrkB (1:1000; BD Biosciences).

436

Immunofluorescence

438 Cells were fixed in 4% PFA and permeabilized with 0.25% Triton-X. Blocking and antibody

439 incubation was performed with Superblock (Thermo Fisher Scientific). Primary antibodies

440 were incubated over night at 4ºC and secondary antibodies for 2h at room temperature. For

441 mouse brain tissue immunofluorescence, sections were washed with PBS and incubated for

442 30 min in NH$_4$Cl. Next, sections were blocked with 0.3% Triton-100 10% NGS in PBS for 2h

443 prior incubation with the primary antibodies diluted in blocking solution overnight at 4ºC.

444 Later, sections were washed and incubated for 2h with the secondary antibodies. Slices

445 were then washed with PBS. Both cells and tissue samples were mounted with Prolong Gold

446 antifade mountant (Thermo Fisher Scientific). The following antibodies were used: GFP

447 (1:500), SV2a (1:100) (both from Santa Cruz Biotechnology), PSD-95 (1:50; Thermo Fisher

448 Scientific), GluA1 (1:250-1:500; Merck Millipore) and RTP801 (1:100; Proteintech).

449 AlexaFluor-488 or -555 secondary antibodies (1:500) and Hoechst33342 (1:5000) were from

450 Thermo Fisher Scientific. Images were obtained with a Leica LCS SL or a Zeiss LSM880

451 confocal microscopes with a 1024x1024 pixel resolution and a 63x magnification and were

452 analyzed with ImageJ. For in vitro experiments in cortical neurons, at least 25 dendrites per

453 group from three independent experiments were analyzed. For in vitro experiments in

454 hippocampal neurons, at least 12 neurons per group were analyzed from three independent

455 experiments. For double-labeled GluA1-PSD-95-positive clusters in brain slices, images

16

456 were acquired with 4x digital zoom (33.74x33.74 μm). For each mouse three representative

457 images from two different coronal sections were analyzed. Colocalization was considered

458 when there was at least one common pixel between GluA1 and PSD-95 detected puncta.

459

460 **Nissl staining**

461 Slices were stained for 45 min with 0.2 mg/ml Cresyl violet (Sigma) in a 0.1 M acetic acid 0.1

462 M sodium acetate solution. Next, slices were washed in distilled water and then dehydrated

463 with ethanol (70, 95, 100%, 5 minutes each), washed with xylol and mounted with DPX

464 media. Images were obtained with a 10x magnification with a Zeiss Axiolab.

465

466 **Behavioral assessment**

467 **Footprint test:** Mice's fore and hindlimbs were painted in blue and red, respectively, with

468 non-toxic ink. Animal's gait was then recorded letting them walk through a tunnel on white

469 paper (10 cm wide, 40 cm long). The test was performed three times on the same day. In

470 each trial three consecutive steps were measured for each parameter (stride, sway, stance,

471 overlap).

472 Open field test: mice were placed in a 40x40x40 cm arena. The center area was considered

473 as the central squared 20x20 cm space. Light intensity was 24 lux though-out the periphery

474 and 29 lux in the center. Mice's movement was tracked and recorded for 10 minutes using

475 SMART 3.0 Software (Panlab). Other parameters related to anxiety-like behaviors, like

476 number of groomings, rearings and defecations were also monitored.

477 **Accelerating rotarod:** one day after the Open field test mice were subjected to the

478 Accelerating rotarod test. Mice were placed on a 3 cm rod with an increasing speed from 4

479 to 40 rpm over 5 minutes. Latency to fall was recorded as the time mice spent in the rod

480 before falling. Accelerating rotarod test was performed for 4 days, 4 trials per day. Trials in

481 the same day were separated by 1 hour.

482 **Clasping behavior:** Hindlimb clasping was measured by picking up mice at the base of the

483 tail. In order to classify this phenotype we used the scale described in (Guyenet *et al*, 2010)

17

484   with minor modifications: 0 means no hind paw retraction, 1, one hindlimb retracted, 2, both

485   hindlimbs partially retracted, and 3 when the 2 hindlimbs were totally retracted.

486

487   **Golgi Staining and spine density and morphology analyses**

488   Golgi-Cox impregnation was performed with fresh brain hemispheres from, mice sacrificed

489   one week after behavioral testing with FD Rapid GolgiStain^{TM}kit (FD Neurotechnologies)

490   following manufacturer's instructions. 100 μm slices were obtained with a Leica vibratome

491   and mounted on gelatin-coated slides before final staining.

492   For spine density analyses only pyramidal neurons from layer V in the primary motor cortex

493   or medium spiny neurons (MSNs) from the dorsolateral striatum were taken into account.

494   Spine density was quantified in dendritic segments of at least 10 μm and 30 different

495   secondary/tertiary dendrites per animal were analyzed. Analyzed dendrites were 50% apical,

496   50% basal.

497   Spine morphology analyses were performed in motor cortex layer V pyramidal neurons.

498   Spines in 5 apical and 5 basal secondary/tertiary dendrites were analyzed for each animal (6

499   WT and 4 KO), in segments of at least 10 μm long. A total of 100-125 apical and 100-125

500   basal spines were analyzed per animal. Branched, filopodia and stubby spines were visually

501   categorized. For headed spines, head area was measured in all headed spines and

502   thin/mushroom classification was performed depending on the mean head area for each

503   genotype (spines with head area greater than the mean were considered as mushroom

504   spines and smaller ones were categorized as thin spines). In spine density and morphology

505   analyses, animal genotype was blind for the experimenter.

506

507   **Transmission electron microscopy**

508   2 months old RTP801 knock out (n=4) and wild type mice (n=4) were sacrificed one week

509   after behavioral testing and motor cortex was dissected from coronal sections. From these

510   sections, the lower half of the motor cortex, including Layer V and VI, was isolated and fixed

511   overnight in 2% glutaraldehyde 2% paraformaldehyde in 0.12 M phosphate buffer. After

512   fixation, tissue was processed and analyzed as previously described in (Bosch *et al*, 2016).

513   Electron micrographs were randomly taken at 25.000x with a TEM JEOL J1010 (tungsten

514   filament), with a CCD Orius (Gatan) and software Digital Micrograph (Gatan). Spine density,

515   pre/postsynaptic area and postsynaptic density area, length and thickness were determined

516   (n=45-50 images for each animal) with ImageJ software. In all TEM analyses, animal

517   genotype was blind for the experimenter.

518

519   **Electrophysiology**

520   **Rat neuronal cultures:** miniature excitatory postsynaptic currents (mEPSCs) were

521   measured in rat primary hippocampal neurons plated on glass coverslips as previously

522   described (Gilbert *et al*, 2016).

523   **Mouse cortical cultures:** Electrophysiological recordings of cultured cortical pyramidal

524   neurons –chosen in basis of their characteristic pyramidal morphology– were performed at

525   14 DIV. Whole-cell patch-clamp currents were recorded at room temperature (25–26 °C) in

526   extracellular solution containing (in mM): 130 NaCl, 3.5 KCl, 10 HEPES, 15 glucose and 2

527    $CaCl_2$ (pH 7.4; osmolarity 305 mOsm/Kg with sorbitol). AMPAR-mediated miniature

528   excitatory postsynaptic currents (mEPSCs) were isolated adding to the extracellular solution

529   1µM tetrodotoxin to block evoked synaptic transmission, 100µM picrotoxin to block

530    $GABA_A$ receptors and 50µM APV to block NMDA receptors. Recording electrodes were

531   fabricated from borosilicate glass with a final resistance of 4–5 MΩ and filled with an internal

532   solution containing (in mM): 120 K-Gluconate, 16 KCl, 8 NaCl, 10 HEPES, 0.2 ethylene

533   glycol tetraacetic acid (EGTA), 2 MgATP, 0.3 Na_2GTP (pH 7.2; osmolarity 291 with sorbitol).

534   Recordings were acquired at a sampling rate of 5KHz and were filtered at 2Hz. Miniature

535   events were detected and analyzed with the WaveMetrics Igor Pro open-source software

536   package Neuromatic (Rothman & Silver, 2018). Frequency was determined by dividing the

537   number of detected events by the recorded time (in seconds).

538

Electrophysiological field recordings

Two-month old (female and male) mouse brain sagittal sections were obtained on a vibratome (Microm HM 650 V, Thermo Scientific, Waltham, MA, USA) at 350 µm thickness in oxygenated (95% O_2, 5% CO_2) ice-cold aCSF and then transferred to a oxygenated 32°C recovery solution for 15 min as previously described (Choi *et al*, 2019). Then, slices were transferred to oxygenated aCSF at room temperature and left for at least 1 h before electrophysiological field recording. Following recovery, mouse 350 µm thick brain slices were placed in a multi electrode array (MEA) recording dish and fully submerged in oxygenated aCSF at 37 °C. Electrophysiological data were recorded with a MEA set-up from Multi Channel Systems MCS GmbH (Reutlingen, Germany) composed of a 60 channels USB-MEA60-inv system. Experiments were carried out with 60MEA200/30iR-ITO MEA dishes consisting of 60 planar electrodes (30 µm diameter) arranged in an 8x8 array and placed in the motor cortex slice surface. Raw traces were recorded for 5 min from 58 electrodes simultaneously, sampled at 5 kHz. Raw data were high-pass filtered with a 200-Hz Butterworth 2nd order filter, the noise level calculated by the standard deviation of the recorded signal on each electrode and spikes were identified as currents with a negative amplitude larger than -30 mV and slope values between 0.2 and 1. To quantify burst activity in spike-trains we applied the MaxInterval Method (Legendy & Salcman, 1985) with the following parameter values: maximum beginning ISI, 200 ms; maximum end ISI, 200 ms; minimum interburst interval, 20 ms, minimum burst duration 20 ms; minimum number of spikes in a burst, 5. Software for recording and signal processing was MC Rack from Multi Channel Systems. Using a digital camera during recording assessed the position of the brain slices on the electrode field to analyze information from electrodes specifically positioned on cortical layer V (**Fig 2 H**).

Experimental design and statistical analyses

20

565   Graphs show results reported as mean±SEM. Data was assessed for normality using

566   D'Agostino-Pearson, Shapiro-Wilk or Kolmogorov-Smirnov. Statistical analyses were

567   performed using unpaired, two-tailed Student's T-test for normally distributed data, Mann-

568   Whitney test for non-parametric data and Two-way ANOVA followed by Bonferroni's *post-*

569   *hoc* tests to compare multiple groups, as appropriate and indicated in the figure legends.

570   Values of *P*< 0.05 were considered as statistically significant.

571   **Ethical Approval and Consent to participate:**

572   All procedures were performed in compliance with the NIH Guide for the Care and Use of

573   Laboratory Animals and approved by the local animal care committee of Universitat de

574   Barcelona following European (2010/63/UE) and Spanish (RD53/2013) regulations for the

575   care and use of laboratory animals.

576   Human samples were obtained following the guidelines and approval of the local ethics

577   committee (Hospital Clínic of Barcelona's Clinical Research Ethics Committee).

578

579

595

AUTHOR CONTRIBUTION:

597   L.P-S., N.M-F., M.M., J.S., A.LL., J.R-A., J.S., G.C., M.C., D.S., X.G., J.A and C.M. have

598   contributed in the conception and design of the study, acquisition and analysis of data and in

599   drafting the manuscript and figures. G.C., E.G-G., N.S-F., S.F-G., J.P.G., M.J.R., H-Y.M.,

600   E.F. and D.W., have contributed in acquisition and analysis of data and in drafting the

601   manuscript and figures.

602

CONFLICT OF INTERESTS: None

604

605

606

REFERENCES:

608   Anderson CT, Sheets PL, Kiritani T & Shepherd GMG (2010) Sublayer-specific microcircuits

609   of corticospinal and corticostriatal neurons in motor cortex. *Nat Neurosci* 13: 739–744

610   Arellano JI, Benavides-Piccione R, Defelipe J & Yuste R (2007) Ultrastructure of dendritic

611   spines: correlation between synaptic and spine morphologies. *Front Neurosci* 1: 131–

612   43

613   Béïque JC & Andrade R (2003) PSD-95 regulates synaptic transmission and plasticity in rat

614   cerebral cortex. *J Physiol* 546: 859–867 doi:10.1113/jphysiol.2002.031369 [PREPRINT]

615   Bosch C, Muhaisen A, Pujadas L, Soriano E & Martínez A (2016) Reelin Exerts Structural,

616   Biochemical and Transcriptional Regulation Over Presynaptic and Postsynaptic

617   Elements in the Adult Hippocampus. *Front Cell Neurosci* 10: 138

618   Brafman A, Mett I, Shafir M, Gottlieb H, Damari G, Gozlan-Kelner S, Vishnevskia-Dai V,

619   Skaliter R, Einat P, Faerman A, *et al* (2004) Inhibition of oxygen-induced retinopathy in

620   RTP801-deficient mice. *Invest Ophthalmol Vis Sci* 45: 3796–3805

621 Calabresi P, Centonze D, Gubellini P, Marfia GA, Pisani A, Sancesario G & Bernardi G

622   (2000) Synaptic transmission in the striatum: from plasticity to neurodegeneration. *Prog*

623   *Neurobiol* 61: 231–65

624 Calabresi P, Galletti F, Saggese E, Ghiglieri V & Picconi B (2007) Neuronal networks and

625   synaptic plasticity in Parkinson's disease: beyond motor deficits. *Park Relat Disord* 13

626   Suppl 3: S259-62

627 Canal M, Martín-Flores N, Pérez-Sisqués L, Romaní-Aumedes J, Altas B, Man H-Y, Kawabe

628   H, Alberch J & Malagelada C (2016) Loss of NEDD4 contributes to RTP801 elevation

629   and neuron toxicity: implications for Parkinson's disease. *Oncotarget*

630 Choi K, Holly EN, Davatolhagh MF, Beier KT & Fuccillo M V. (2019) Integrated anatomical

631   and physiological mapping of striatal afferent projections. *Eur J Neurosci* 49: 623–636

632 Chou AH, Yeh TH, Ouyang P, Chen YL, Chen SY & Wang HL (2008) Polyglutamine-

633   expanded ataxin-3 causes cerebellar dysfunction of SCA3 transgenic mice by inducing

634   transcriptional dysregulation. *Neurobiol Dis* 31: 89–101

635 Costa RM, Cohen D & Nicolelis MAL (2004) Differential corticostriatal plasticity during fast

636   and slow motor skill learning in mice. *Curr Biol* 14: 1124–1134

637 Creus-Muncunill J, Rué L, Alcalá-Vida R, Badillos-Rodríguez R, Romaní-Aumedes J, Marco

638   S, Alberch J, Perez-Otaño I, Malagelada C & Pérez-Navarro E (2018) Increased Levels

639   of Rictor Prevent Mutant Huntingtin-Induced Neuronal Degeneration. *Mol Neurobiol*

640 Fu M, Yu X, Lu J & Zuo Y (2012) Repetitive motor learning induces coordinated formation of

641   clustered dendritic spines in vivo. *Nature* 483: 92–96

642 Gilbert J, Shu S, Yang X, Lu Y, Zhu L-Q & Man H-Y (2016) β-Amyloid triggers aberrant over-

643   scaling of homeostatic synaptic plasticity. *Acta Neuropathol Commun* 4: 131

644 Guo L, Xiong H, Kim J-I, Wu Y-W, Lalchandani RR, Cui Y, Shu Y, Xu T & Ding JB (2015)

645   Dynamic rewiring of neural circuits in the motor cortex in mouse models of Parkinson's

646   disease. *Nat Neurosci* 18: 1299–1309

647 Guo W, Ji Y, Wang S, Sun Y & Lu B (2014) Neuronal activity alters BDNF-TrkB signaling

648   kinetics and downstream functions. *J Cell Sci* 127: 2249–60

649 Guyenet SJ, Furrer SA, Damian VM, Baughan TD, La Spada AR & Garden GA (2010) A

650   Simple Composite Phenotype Scoring System for Evaluating Mouse Models of

651   Cerebellar Ataxia. *J Vis Exp*

652 Hintiryan H, Foster NN, Bowman I, Bay M, Song MY, Gou L, Yamashita S, Bienkowski MS,

653   Zingg B, Zhu M, *et al* (2016) The mouse cortico-striatal projectome. *Nat Neurosci* 19:

654   1100–1114

655 Kabir ZD, Lee AS, Burgdorf CE, Fischer DK, Rajadhyaksha AM, Mok E, Rizzo B, Rice RC,

656   Singh K, Ota KT, *et al* (2017) Cacna1c in the Prefrontal Cortex Regulates Depression-

657   Related Behaviors via REDD1. *Neuropsychopharmacology* 42: 2032–2042

658 Kida H, Tsuda Y, Ito N, Yamamoto Y, Owada Y, Kamiya Y & Mitsushima D (2016) Motor

659   Training Promotes Both Synaptic and Intrinsic Plasticity of Layer II/III Pyramidal

660   Neurons in the Primary Motor Cortex. *Cereb Cortex* 26: 3494–3507

661 Labadorf A, Choi SH & Myers RH (2018) Evidence for a Pan-Neurodegenerative Disease

662   Response in Huntington's and Parkinson's Disease Expression Profiles. *Front Mol*

663   *Neurosci* 10: 430

664 Lauterborn JC, Lynch G, Vanderklish P, Arai A & Gall CM (2000) Positive modulation of

665   AMPA receptors increases neurotrophin expression by hippocampal and cortical

666   neurons. *J Neurosci* 20: 8–21

667 Lee A, Hirabayashi Y, Kwon SK, Lewis TL & Polleux F (2018) Emerging roles of

668   mitochondria in synaptic transmission and neurodegeneration. *Curr Opin Physiol* 3: 82–

669   93 doi:10.1016/j.cophys.2018.03.009 [PREPRINT]

670 Legendy CR & Salcman M (1985) Bursts and recurrences of bursts in the spike trains of

671   spontaneously active striate cortex neurons. *J Neurophysiol* 53: 926–939

672 Lu W, Shi Y, Jackson AC, Bjorgan K, During MJ, Sprengel R, Seeburg PH & Nicoll RA

673   (2009) Subunit Composition of Synaptic AMPA Receptors Revealed by a Single-Cell

674   Genetic Approach. *Neuron* 62: 254–268

675 Malagelada C, Lopez-Toledano MA, Willett RT, Jin ZH, Shelanski ML & Greene LA (2011)

676   RTP801/REDD1 regulates the timing of cortical neurogenesis and neuron migration. *J*

677   *Neurosci* 31: 3186–3196

678 Malagelada C, Ryu EJ, Biswas SC, Jackson-Lewis V & Greene LA (2006) RTP801 is

679   elevated in Parkinson brain substantia nigral neurons and mediates death in cellular

680   models of Parkinson's disease by a mechanism involving mammalian target of

681   rapamycin inactivation. *J Neurosci* 26: 9996–10005

682 Malagelada C, Zong HJ & Greene LA (2008) RTP801 is induced in Parkinson's disease and

683   mediates neuron death by inhibiting Akt phosphorylation/activation. *J Neurosci* 28

684 Man H-Y (2011) GluA2-lacking, calcium-permeable AMPA receptors — inducers of

685   plasticity? *Curr Opin Neurobiol* 21: 291–298

686 Mangiarini L, Sathasivam K, Seller M, Cozens B, Harper A, Hetherington C, Lawton M,

687   Trottier Y, Lehrach H, Davies SW, *et al* (1996) Exon I of the HD gene with an expanded

688   CAG repeat is sufficient to cause a progressive neurological phenotype in transgenic

689   mice. *Cell* 87: 493–506

690 Martín-Flores N, Pérez-Sisqués L, Creus-Muncunill J, Masana M, Ginés S, Alberch J, Pérez-

691   Navarro E & Malagelada C (2020) Synaptic RTP801 contributes to motor-learning

692   dysfunction in Huntington's disease. *Cell Death Dis* 11: 1–15

693 Martín-Flores N, Romaní-Aumedes J, Rué L, Canal M, Sanders P, Straccia M, Allen ND,

694   Alberch J, Canals JM, Pérez-Navarro E, *et al* (2016) RTP801 Is Involved in Mutant

695   Huntingtin-Induced Cell Death. *Mol Neurobiol* 53: 2857–2868

696 Martin-Flores N, Romani-Aumedes J, Rue L, Canal M, Sanders P, Straccia M, Allen

697   NDDNDNDD, Alberch J, Canals JM, Perez-Navarro E, *et al* (2015) RTP801 Is Involved

698   in Mutant Huntingtin-Induced Cell Death. *Mol Neurobiol* 53: 2857–2868

699 Meyer D, Bonhoeffer T & Scheuss V (2014) Balance and stability of synaptic structures

700   during synaptic plasticity. *Neuron* 82: 430–443

701 Noseda R, Belin S, Piguet F, Vaccari I, Scarlino S, Brambilla P, Martinelli Boneschi F, Feltri

702   ML, Wrabetz L, Quattrini A, *et al* (2013) DDIT4/REDD1/RTP801 is a novel negative

703   regulator of Schwann cell myelination. *J Neurosci* 33: 15295–305

704   Ota KT, Liu RJ, Voleti B, Maldonado-Aviles JG, Duric V, Iwata M, Dutheil S, Duman C,

705   Boikess S, Lewis DA, *et al* (2014) REDD1 is essential for stress-induced synaptic loss

706   and depressive behavior. *Nat Med* 20: 531–535

707   Ozcan AS (2017) Filopodia: A Rapid Structural Plasticity Substrate for Fast Learning. *Front*

708   *Synaptic Neurosci* 9: 12

709   Peters AJ, Liu H & Komiyama T (2017) Learning in the Rodent Motor Cortex. *Annu Rev*

710   *Neurosci* 40: 77–97

711   Romani-Aumedes J, Canal M, Martin-Flores N, Sun X, Perez-Fernandez V, Wewering S,

712   Fernandez-Santiago R, Ezquerra M, Pont-Sunyer C, Lafuente A, *et al* (2014) Parkin

713   loss of function contributes to RTP801 elevation and neurodegeneration in Parkinson's

714   disease. *Cell Death Dis* 5: e1364

715   Romaní-Aumedes J, Canal M, Martín-Flores N, Sun X, Pérez-Fernández V, Wewering S,

716   Fernández-Santiago R, Ezquerra M, Pont-Sunyer C, Lafuente A, *et al* (2014) Parkin

717   loss of function contributes to RTP801 elevation and neurodegeneration in Parkinson's

718   disease. *Cell Death Dis* 5

719   Roth RH, Cudmore RH, Tan HL, Hong I, Zhang Y & Huganir RL (2020) Cortical Synaptic

720   AMPA Receptor Plasticity during Motor Learning. *Neuron* 105: 895-908.e5

721   Rothman JS & Silver RA (2018) NeuroMatic: An Integrated Open-Source Software Toolkit

722   for Acquisition, Analysis and Simulation of Electrophysiological Data. *Front Neuroinform*

723   12

724   Ryu EJ, Angelastro JM & Greene LA (2005) Analysis of gene expression changes in a

725   cellular model of Parkinson disease. *Neurobiol Dis* 18: 54–74

726   Sanes JN & Donoghue JP (2000) Plasticity and Primary Motor Cortex. *Annu Rev Neurosci*

727   23: 393–415

728   Shepherd GMG (2013) Corticostriatal connectivity and its role in disease. *Nat Rev Neurosci*

729   14: 278–291 doi:10.1038/nrn3469 [PREPRINT]

730   Shepherd JD & Huganir RL (2007) The Cell Biology of Synaptic Plasticity: AMPA Receptor

731   Trafficking. *Annu Rev Cell Dev Biol* 23: 613–643

732   Shoshani T, Faerman A, Mett I, Zelin E, Tenne T, Gorodin S, Moshel Y, Elbaz S, Budanov

733   A, Chajut A, *et al* (2002) Identification of a novel hypoxia-inducible factor 1-responsive

734   gene, RTP801, involved in apoptosis. *Mol Cell Biol* 22: 2283–2293

735   Tjia M, Yu X, Jammu LS, Lu J & Zuo Y (2017) Pyramidal Neurons in Different Cortical

736   Layers Exhibit Distinct Dynamics and Plasticity of Apical Dendritic Spines. *Front Neural*

737   *Circuits* 11: 43

738   Todorova V & Blokland A (2017) Mitochondria and Synaptic Plasticity in the Mature and

739   Aging Nervous System. *Curr Neuropharmacol* 15: 166–173

740   Xu T, Wang S, Lalchandani RR & Ding JB (2017) Motor learning in animal models of

741   Parkinson's disease: Aberrant synaptic plasticity in the motor cortex. *Mov Disord* 32:

742   487–497

743   Xu T, Yu X, Perlik AJ, Tobin WF, Zweig JA, Tennant K, Jones T & Zuo Y (2009) Rapid

744   formation and selective stabilization of synapses for enduring motor memories. *Nature*

745   462: 915–919

746   Yuste R, Majewska A & Holthoff K (2000) From form to function: calcium

747   compartmentalization in dendritic spines. *Nat Neurosci* 3: 653–659

748   Zhang Z, Chu S-F, Wang S-S, Jiang Y-N, Gao Y, Yang P-F, Ai Q-D & Chen N-H (2018)

749   RTP801 is a critical factor in the neurodegeneration process of A53T α-synuclein in a

750   mouse model of Parkinson's disease under chronic restraint stress. *Br J Pharmacol*

751   175: 590–605

752   Ziv NE & Smith SJ (1996) Evidence for a role of dendritic filopodia in synaptogenesis and

753   spine formation. *Neuron* 17: 91–102

754   Zuo Y, Lin A, Chang P & Gan W-B (2005) Development of Long-Term Dendritic Spine

755   Stability in Diverse Regions of Cerebral Cortex. *Neuron* 46: 181–189

756

757

758   **ABBREVIATIONS**:

759   Alzheimer's disease (AD); Huntington's disease (HD); knock out (KO); mechanistic target of

760   rapamycin (mTOR); primary motor cortex (M1), motor cortex layer V (LV); mutant huntingtin

761   (mhtt); microelectrode arrays (MEAs); miniature excitatory postsynaptic currents (mEPSC);

762   Parkinson's disease (PD); induced pluripotent stem cells (iPSC); postsynaptic density

763   (PSD); transmission electron microscopy (TEM); tuberous sclerosis complex (TSC1/2);

764   substantia nigra pars compacta (SNpc); wild type (WT).

765

766

767   **FIGURE LEGENDS:**

768   **Figure 1. RTP801 is present at the synapse and modulates neuronal transmission. A.**

769   **RTP801 protein is found in the synaptic compartment.** Homogenate (H) and crude

770   synaptic fraction (S) were obtained from human *postmortem cortex (CTX) and putamen*

771   *(STR),* adult rat cortex (CTX) and striatum (STR), primary cortical cultures at 14 DIVs and

772   cortex from both 2-months old WT and RTP801 KO mice. Whole cell lysate (L) from NGF-

773   differentiated PC12 cells was added as a positive control to detect RTP801 in mouse brains.

774   Samples were analyzed by western blot and proved against RTP801 (specific band pointed

775   out by *), postsynaptic protein PSD-95 and actin as a loading control. **B. RTP801 is present**

776   **ubiquitously in neurons, including at the synapses.** Primary rat cortical cultures were

777   fixed at 14DIVs and stained for RTP801 (grey). Phalloidin (red) was used to visualize actin

778   cytoskeleton. Nuclei were stained with Hoechst33342 (in blue). White arrows point F-actin-

779   labeled dendritic spines colocalizing with endogenous RTP801 staining. **C. RTP801**

780   **knockdown reduces spine density in cultured cortical neurons.** Primary rat cortical

781   neurons were transduced with lentiviral particles carrying a GFP-tagged control shRNA or an

782   shRNA against RTP801. 4 days later (14 DIVs), cells were fixed and analyzed by

783   immunofluorescence against GFP (green). *Scale bar, 5µm.* **D. Abrogation of RTP801**

784   **expression modulates synaptic plasticity *in vitro.* D.1.** Representative 20 seconds

785   whole-cell recording of mEPSCs at a membrane voltage of –70mV from WT or RTP801 KO

786   mice cultured cortical pyramidal neurons (14 DIV). A magnification (0.5 seconds) for both

28

787 traces is shown below where asterisks denote the detected events. **D.2.** Example of

788 averaged mEPSCs (red lines) superimposed on the individual mEPSCs (in black) from a

789 wild type (average of 962 events) and RTP801 knockout (average of 236 events) culture.

790 **D.3.** RTP801 KO recordings show differences in mEPSCs mean amplitude. **D.4.** The

791 frequency of detected events in RTP801 KO neurons was statistically increased compared

792 with WT. mEPSCs frequencies were obtained from same recordings shown in D.3. All data

793 is presented as mean ± SEM from the recordings performed in 15 WT neurons and 25 KO

794 neurons from at least six independent neuronal cultures. Statistical analyses for spine

795 density and mEPSC amplitude were performed with Student's t-test, *P< 0.05, ***P0.001 vs.

796 shCt/WT and with Mann-Whitney test for mEPSC frequency, *P<0.05 vs. WT.

797

798 **Figure 2. RTP801 KO mice show decreased brain size, decreased cortical spine**

799 **density and enhanced synaptic transmission.**

800 **A.** Whole brain extracts from WT and RTP801 KO mice at 2 months of age were subjected

801 to western blot. Membranes were proved against RTP801 (specific band is pointed out by *)

802 and actin as loading control. **B.** 9-weeks long follow-up shows that RTP801 KO animals

803 display normal weight. **C.** RTP801 KO mice exhibit decreased brain weight. Whole brain

804 weight was measured in 2-months-old animals. **D**. Brain sections of WT and KO mice were

805 subjected to Nissl staining to visualize cell somas. Representative images of motor cortex

806 (CTX), hippocampus (HIP) and striatum (STR) for both genotypes are shown. *Scale bar*,

807 250μm. Motor cortex thickness (**E**) and LV cell density (**F**) were quantified in Nissl-stained

808 sections. **G**. RTP801 total knockout mice show decreased spine density in motor cortex

809 layer V. Spine density was quantified in 30 dendrites/animal, 50% apical and 50% basal, in 5

810 WT and 5 KO animals. *Scale bar,* 10 μm. **H.** Image of a brain sagittal slice on the MEA

811 (magnification). Recordings from the selected electrodes (in red), located on LV, were

812 analyzed. Motor cortex layers I-VI and *corpus callosum* (CC) are indicated. *Scale bar,* 600

813 μm. **I.** Spontaneous activity by MEA: Illustrative long time-scale (90 min) spike rasters of

814 recorded LV motor cortex spontaneous activity from WT (4 males and 3 females) and

815   RTP801 KO (4 males and 4 females) mouse brain slices (1 slice per animal); the horizontal

816   lines above each raster define bursts. Graphs show quantification of spike rate (**I.1**), burst

817   rate (**I.2**), and the percent of spikes that form bursts (**I.3**) of field spontaneous activity

818   recorded by MEA. Data in all graphs are presented as mean ± SEM. * $P<0.05$, ***$P<0.001$;

819   two-tailed Student t-test *versus* WT (**C**, **F**). *$P<0.05$; Mann-Whitney test versus WT (**I.1-I.3**).

820   Data in (**B, E**) was analyzed by two-way ANOVA.

821

822   **Figure 3. RTP801 contributes to motor learning and gait but does not alter general**

823   **locomotor activity. A.** Schematic representation of the four different parameters measured

824   in the footprint test: stride, sway, stance and limbs overlap (in blue, forelimb prints and, in

825   red, hindlimb prints). **B.** Representative examples of footprint tracking from both genotypes.

826   Graphs on the right show hindlimb lengths for stride, sway, stance and limbs overlap. Data is

827   represented as mean ± SEM and was analyzed with two-tailed Student's t-test. * $P< 0.05$, **

828    $P< 0.01$, *** $P< 0.001$ *versus* WT group. N = 13 WT (8 males + 5 females) and 12 KO (4

829   males + 8 females). **C.** Representative tracking of mice activity recorded for 10 minutes in an

830   open field test. Graphs on the right show total distance traveled in the whole arena (blue),

831   distance traveled in the center (red) and percentage of time spent in the center. Measures

832   are shown as mean ± SEM. There are no statistically significant differences according to the

833   Student's t-tests performed. N = 18 WT (6 males + 12 females) and 17 KO (7 males + 10

834   females). **D**. WT and RTP801 KO mice were subjected to the accelerating rotarod test and

835   the time spent on it was evaluated for three days, four trials per day. Data is represented as

836   mean ± SEM and was analyzed by two-way ANOVA followed by Bonferroni's multiple

837   comparisons test for *post hoc* analyses. Genotype effect: ** $P< 0.01$. Multiple comparisons: *

838    $P< 0.05$, ** $P< 0.01$, *** $P< 0.001$ *versus* WT group in each trial. N = 31 WT (14 males + 17

839   females) and 30 KO (12 males + 18 females).

840

841   **Figure 4. RTP801 modulates dendritic spine density and morphology of pyramidal**

842   **neurons in M1 in motor-trained animals.** One week after the accelerating rotarod test, WT

843 and RTP801 KO mice were culled and their brains were impregnated with Golgi-Cox

844 staining prior to analyze changes in spine density. **A, B. Loss of RTP801 expression**

845 **decreases spine density of pyramidal neurons from M1.** Spine density was quantified

846 combining both apical and basal dendrites from M1 LV pyramidal neurons. **A**, **C.**

847 **Abrogation of RTP801 expression affects specifically basal dendrites of pyramidal**

848 **neurons in M1.** Spine density was assessed in apical and basal dendrites. Each bar of the

849 graphs represents mean ± SEM of at least 30 dendrites per animal (N= 8 WT and 5 KO),

850 approximately 50% apical and 50% basal. **A, D. Loss of RTP801 expression does not**

851 **affect spine density in the striatum.** Spine density was also analyzed in striatal MSNs.

852 Data in the graph represent mean ± SEM of at least 30 dendrites per animal (N= 8 WT and 5

853 KO). Statistical analyses in a were performed with Mann-Whitney test, **$P<0.01$ vs. WT, and

854 by Two-tailed Student's t-test in c-d; ** $P< 0.01$ *versus* WT. Cortical layers (I, II/III, V, VI),

855 *corpus callosum* (CC) and striatum (STR) are depicted in **A**. Representative WT and KO

856 dendrites from primary motor cortex and striatum are shown (**B, D**). *Scale bar,* 10 μm.

857

858 **Figure 5. RTP801 modulates spine morphology of pyramidal neurons in the motor**

859 **cortex of trained animals.** Golgi-stained brains were processed and spine morphology of

860 pyramidal neurons from M1 layer V were analyzed. Schematic representations show the

861 spine morphologies considered in this study. **A.** RTP801 KO mice show reduced

862 percentages of branched spines but increased percentage of filopodia spines in layer V

863 neurons. Graphs show the percentage of each morphological type of dendritic spines *versus*

864 total number of spines analyzed. Percentage of apical and basal thin (**B.1**) and mushroom

865 (**C.1**) spines *versus* total number of spines with head. Spine density measures are

866 represented as mean ± SEM of 50 dendrites per genotype (5 animals per genotype, 5 basal

867 and 5 apical dendrites per animal). Apical and basal spines were analyzed separately. Data

868 in **A**, **B**.1 and **C**.1 was analyzed with two-tailed Student's t-test, * $P< 0.05$, ** $P< 0.01$ *versus*

869 WT. Cumulative probability of apical and basal spine head area in thin (**B.2**) and mushroom

870 (**C.2**). Distributions were compared with the Kolmogorov–Smirnov test. Apical and basal

871 spines were analyzed separately. 5 animals/genotype were analyzed, 5 apical and 5 basal

872 dendrites per animal. Spine head area from basal mushroom spines shows significant

873 differences between genotypes, D=0.2747, *P*=0.0021.

874

875 **Figure 6. Synaptic contacts show structural differences between WT and RTP801 KO**

876 **animals in the motor cortex after motor skill training.** Motor cortex lower layers were

877 analyzed by TEM**. A. Postsynaptic area is increased in RTP801 KO mice synaptic**

878 **contacts. B. Postsynaptic density (PSD) area, length and thickness are increased in**

879 **RTP801 KO mice synaptic contacts.** Histograms show mean ± SEM of the different

880 measures analyzed relative to control mean. Images show a representative PSD for each

881 genotype. **C. Increased presence of mitochondria in RTP801 KO synaptic contacts.**

882 Graphs show the percentage of mitochondria found in synaptic contacts (either in the pre- or

883 postsynaptic compartment) and in the presynapses or postsynapses separately. Data is

884 represented as mean percentage ± SEM. Images show representative contacts where a

885 mitochondrion (M) is present in either the presynapse (PRE) or postsynapse (POST). All

886 histograms represent data from 45-50 images per animal, four animals per genotype. Data

887 in a-c represent data relative to WT mean. Data was analyzed with Mann-Whitney test. * *P*<

888 0.05, ** *P*< 0.01, *** *P*< 0.001 *versus* WT control. For all electron micrographs, *Scale bar,*

889 250 nm.

890

891 **Figure 7. RTP801 modulates synaptic composition in the cortex from motor-trained**

892 **mice. A-C. Lack of RTP801 expression decreases PSD-95 levels but increases AMPAR**

893 **subunit GluA1 levels in synaptosomes.** Levels of postsynaptic proteins were analyzed in

894 2-months-old WT and RTP801 KO animals. Crude synaptosomal fractions were obtained

895 from cortical brain lysates and analyzed by western blotting. Representative images of PSD-

896 95 (**A**), GluA1 , GluA2, Stargazin (**B**), GluN2B (**C**) and actin are shown. **D. Lack of RTP801**

897 **expression increases TrkB receptor levels in motor cortex homogenates.** In the same

898 WT and KO samples levels of full length TrkB was assessed by western blotting from

899   homogenates. Representative images of TrkB and actin are shown. Densitometric measures

900   (mean ± SEM) of total levels of PSD-95 and TrkB were relativized against actin and synaptic

901   levels of the different proteins in the synaptic fraction were relativized against synaptic

902   marker PSD-95. **E-H.** M1 LV excitatory postsynaptic characterization in 2-months old WT

903   and RTP801 KO mice after performing behavioral motor tasks. **E.** Quantification of the

904   number of PSD-95, GluA1 and PSD-95/GluA1 positive puncta per field. **F-G**. Quantification

905   of PSD-95 and GluA1 puncta mean area (**F**) and intensity (**G**). Representative confocal

906   images of a double immunofluorescence of PSD-95 and AMPAR subunit GluA1 in the motor

907   cortex layer 5. *Scale bar,* 100 μm. All values appear as mean ± SEM and were analyzed

908   with two-tailed Student's t-test *versus* WT * $P< 0.05$ and **$P<0.01$.

909

910   **Figure 8. RTP801 KO mice show improved motor learning skills accompanied by**

911   **functional and structural differences at a synaptic level.** In comparison to WT mice,

912   RTP801 KO mice show decreased spine density in M1 LV neurons together with an

913   increase in the proportion of filopodia and mushroom-like dendritic spines. At a structural

914   level, we found increased post-synaptic areas and PSD size and increased presence of

915   mitochondria at the synapse in KO primary motor cortex LV together with increased levels of

916   synaptic GluA1 AMPAR subunit.

917

918   **EXPANDED VIEW FIGURE LEGENDS:**

919

920   **Expanded view figure 1. RTP801 is present in the postsynaptic compartment and its**

921   **overexpression alters synaptic transmission and the levels of synaptic proteins in**

922   **primary cultured hippocampal neurons. A. RTP801 protein colocalizes with**

923   **postsynaptic marker PSD-95.** Cells were fixed at DIV 21 and endogenous RTP801 (green)

924   and PSD-95 (red) were analyzed by immunofluorescence. White arrows designate PSD-95

925   and RTP801 colocalizations. *Scale bar,* 5 μm. **B. RTP801 seldom colocalizes with**

926 **presynaptic protein SV2A.** Cells were fixed at DIV 17 and RTP801 (green) and SV2A (red)

927 proteins were analyzed by immunofluorescence. White arrows point SV2A positive

928 presynaptic *puncta,* which does not colocalize with RTP801. *Scale bar,* 5 μm. **C, D. Ectopic**

929 **RTP801 reduces the intensity of PSD-95 and GluA1 at the synaptic contacts.** Neurons

930 were transfected with a vector expressing RTP801 tagged with eGFP (eGFP-RTP801) or

931 with an eGFP control vector (eGFP). Two days following transfection, at DIV 15, neurons

932 were fixed and subjected to immunofluorescent staining against eGFP (green) and PSD-95

933 (**C**) or GluA1 (**D**) (both in red). Images show a representative staining for each protein.

934 Graphs show immunofluorescent integrated intensity and synaptic accumulation density,

935 represented as mean ± SEM from the analysis of at least 12 neurons per group. Data in c
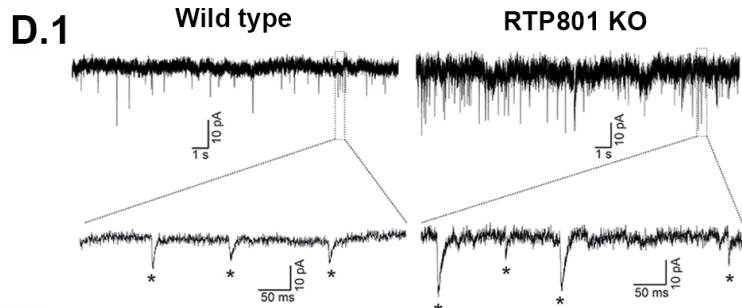
936 was analyzed with two-tailed Student's t-test. Data in d was analyzed with Mann-Whitney

937 test. * $P< 0.05$, ** $P< 0.01$ *vs.* eGFP. *Scale bar,* 10 μm. **F. Ectopic RTP801 attenuates**

938 **postsynaptic excitatory transmission.** Primary cultures of hippocampal neurons from rat

939 E.18 embryos were transfected at DIV 13 with a control vector (eGFP) or a vector

940 expressing RTP801 protein fused with GFP (eGFP-RTP801). Two days later mEPSC were

941 recorded through patch-clamp. Quantitative analysis of mEPSCs amplitude and frequency is

942 represented in the graphics as mean ± SEM from the recordings performed in at least 8

943 transfected neurons per condition. Data was analyzed with Student's t-test, * $P< 0.01$ *vs.*

944 eGFP.

945

946 **Expanded view figure 2. Multielectrode array analysis of M1 LV spontaneous activity**

947 **on mouse slices**. **A**. We found no sex effects in the spike rate differences between WT and

948 RTP801 KO animals (Two-way ANOVA; $F_{(1,11)} = 5.137$; $P = 0.045$; $F_{(1,11)} = 0.374$; for the

949 genotype effect; $P = 0.553$ for the sex effect, $F_{(1,11)} = 1.627$, $P = 0.228$ for the sex/genotype

950 interaction). When we analyzed the spike-train patterns in WT and KO motor cortex slices

951 we found no differences in mean burst duration (**B**), inter-spike interval duration (ISI) inside

952 the bursts (**C**), and spike frequency in the burst (**D**).

34

953

954 **Expanded view figure 3. A. RTP801 KO mice show hindlimb clasping.** Example of

955 clasping reflex; 2-months-old RTP801 KO mice display their hindlimbs towards their

956 abdomen when suspended by the tail. Graphical representation of clasping phenotype

957 scored: 0 (no clasping), 1 (one hindlimb is retracted), 2 (both hindlimbs are partially

958 retracted) and 3 (both hindlimbs totally retracted towards the abdomen). Measures are

959 represented as mean ± SEM and analyzed with two-way ANOVA (genotype effect, *** $P<$

960 0.001) followed by Bonferroni's multiple comparisons test for *post hoc* analyses, *** $P<$

961 0.001. **B. Gait abnormalities are found in both male and female RTP801 KO mice.**

962 Graphics show hindlimb lengths for stride, sway, stance and limbs overlap. Data is

963 represented as mean ± SEM and was analyzed with two-way ANOVA followed by

964 Bonferroni's multiple comparisons test for *post hoc* analyses. * $P<$ 0.05, ** $P<$ 0.01, *** $P<$

965 0.001 *versus* same-gender WT group, N = 8 WT males, 5 WT females, 4 KO males and 8

966 KO females. **C. Anxiety-like behavior analyses during open field test.** The assessment

967 was performed for 10 minutes. Graphs show measures of self-grooming behavior, number of

968 wall and vertical rearings and number of fecal pellets. Data is represented as mean ± SEM

969 and was analyzed with two-way ANOVA followed by Bonferroni's multiple comparisons test

970 for *post hoc* analyses. *** $P<$ 0.001 *versus* same-gender WT group .N = 8 WT males, 5 WT

971 females, 4 KO males and 8 KO females. **D. Both male and female RTP801 KO mice**

972 **display the same tendency to perform better in the Accelerating Rotarod.** Time spent in

973 the accelerating rotarod for three days, four trials per day, by RTP801 KO female and male

974 mice. Data is represented as mean ± SEM and was analyzed with two-way ANOVA. N = 14

975 WT males + 17 WT females and 12 KO males + 18 KO females.

976

977 **Expanded view figure 4. Percentage of different types of spine morphology measured**

978 **in apical and basal dendrites.** Graphs show the percentage of each morphological type of

979 dendritic spines versus total number of spines. Measures are represented as mean ± SEM

980   50 dendrites per genotype (5 animals per genotype, 5 basal and 5 apical dendrites per

981   animal). Data was analyzed with two-tailed Student's t-test, * P<0.05.

982

983   **Expanded view figure 5. A-B.** There are no differences in the number of presynapses and

984   postsynapses with more than one contact between WT and KO animals. Electron

985   micrographs illustrate a presynapse (**A**) with two postsynaptic contacts and a postsynapse

986   (**B**) with two presynaptic inputs. **C.** There are no differences in the percentage of

987   postsynaptic compartments with spine apparatus (S. App) between genotypes. Image on the

988   right show a perforated contact with a spine apparatus in the postsynapse. Data is

989   represented as mean percentage ± SEM. All histograms represent data from 45-50 images

990   per animal, four animals per genotype. Data was analyzed with Student's t-test.

991

992

FIGURE 1
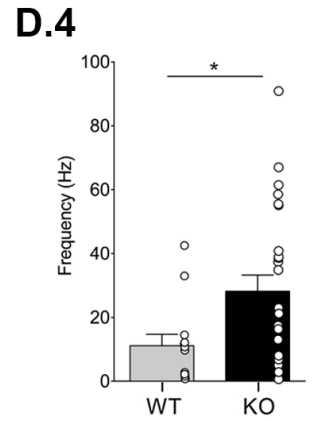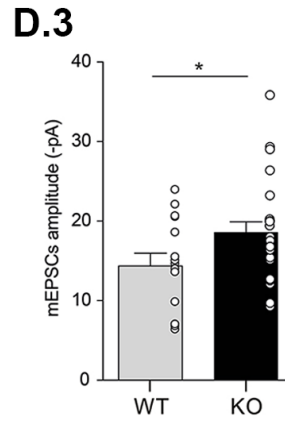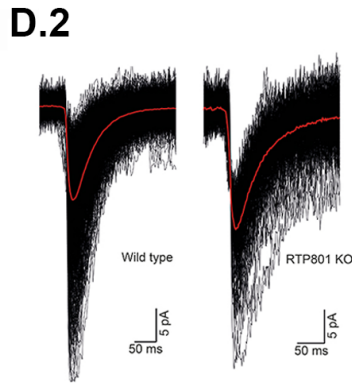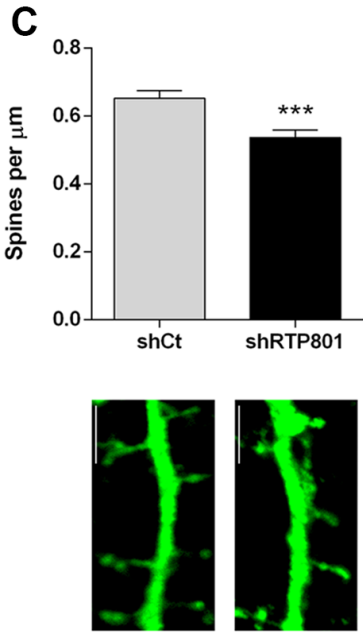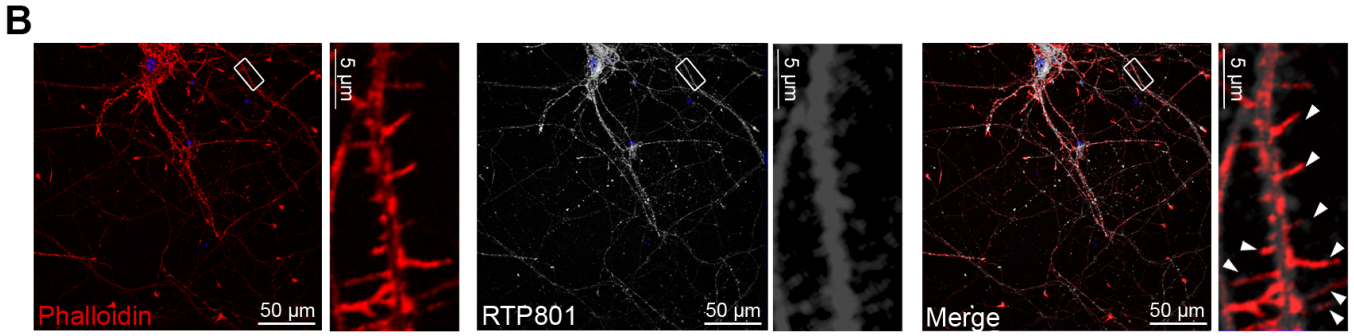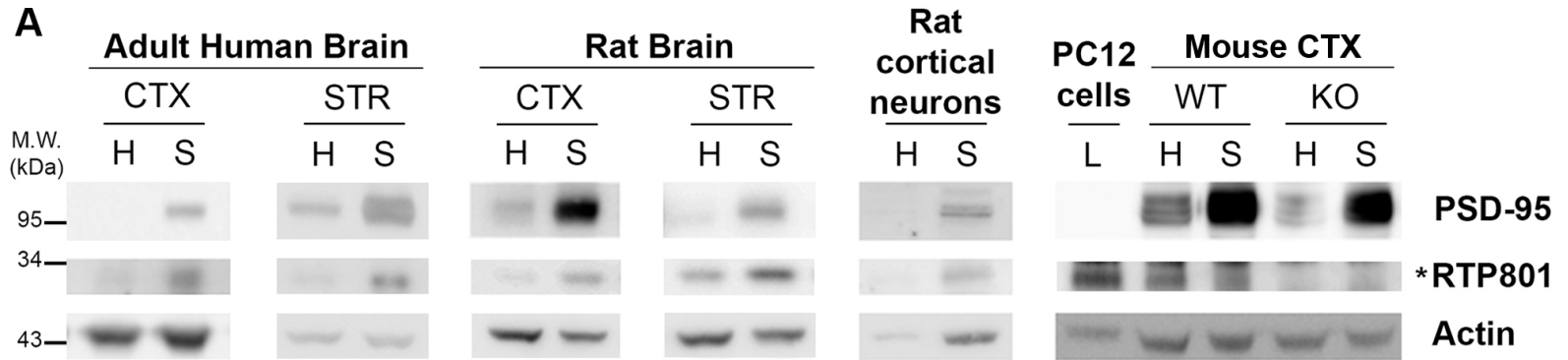
FIGURE 2

FIGURE 3

FIGURE 4

A

B CORTEX - Pyramidal neuron

C Apical dentrites   Basal dendrites

D STRIATUM - Medium spiny neuron
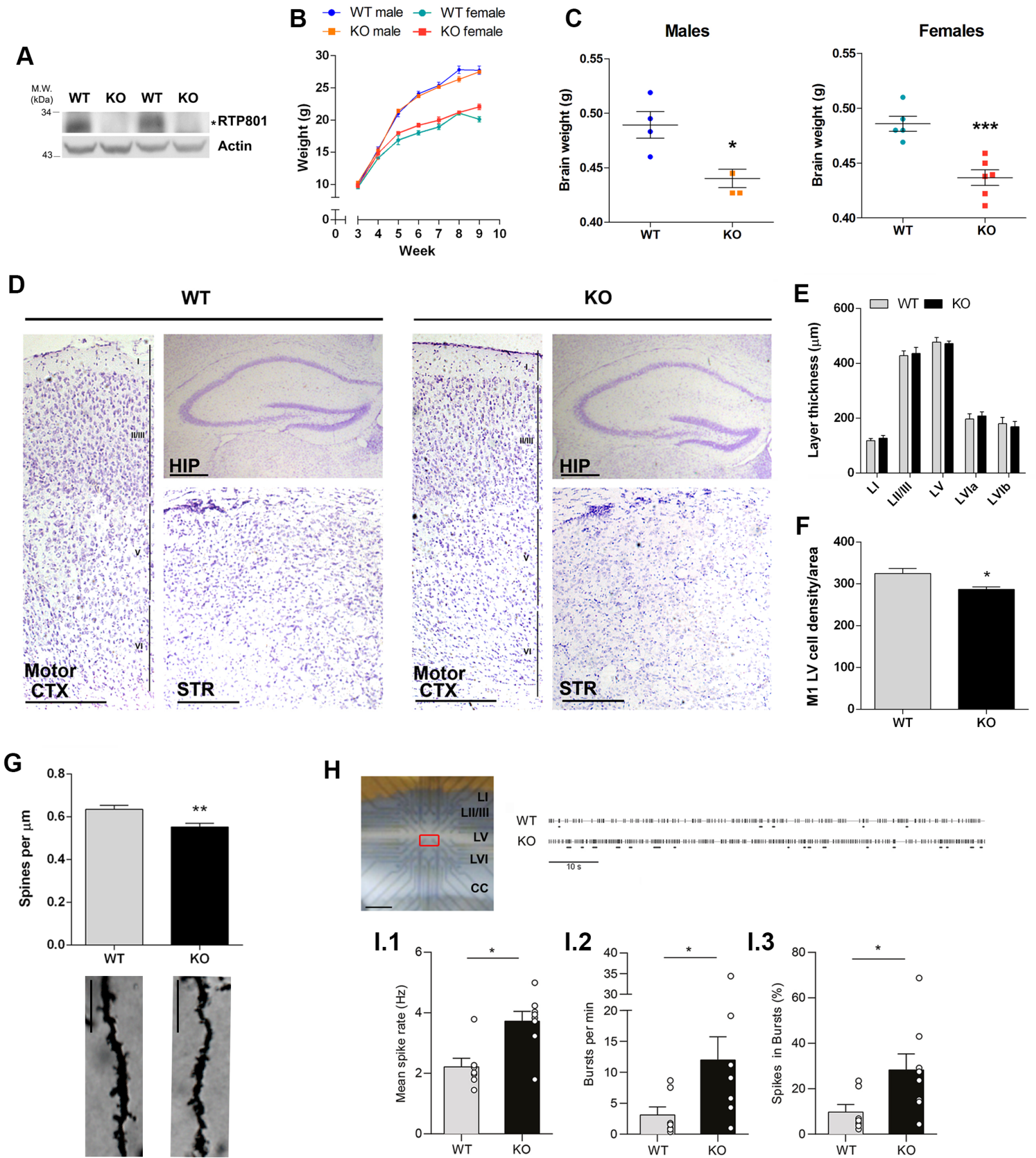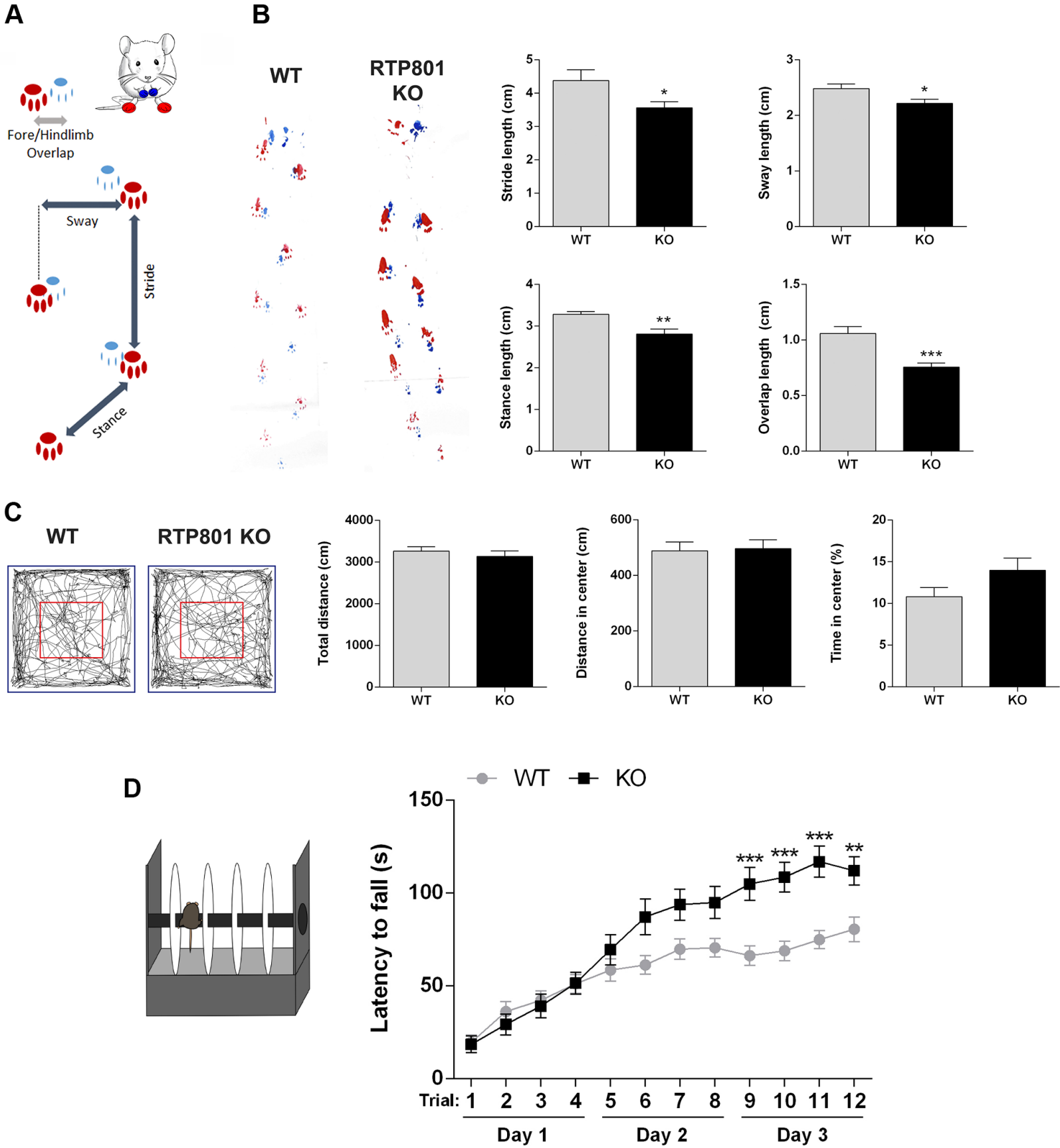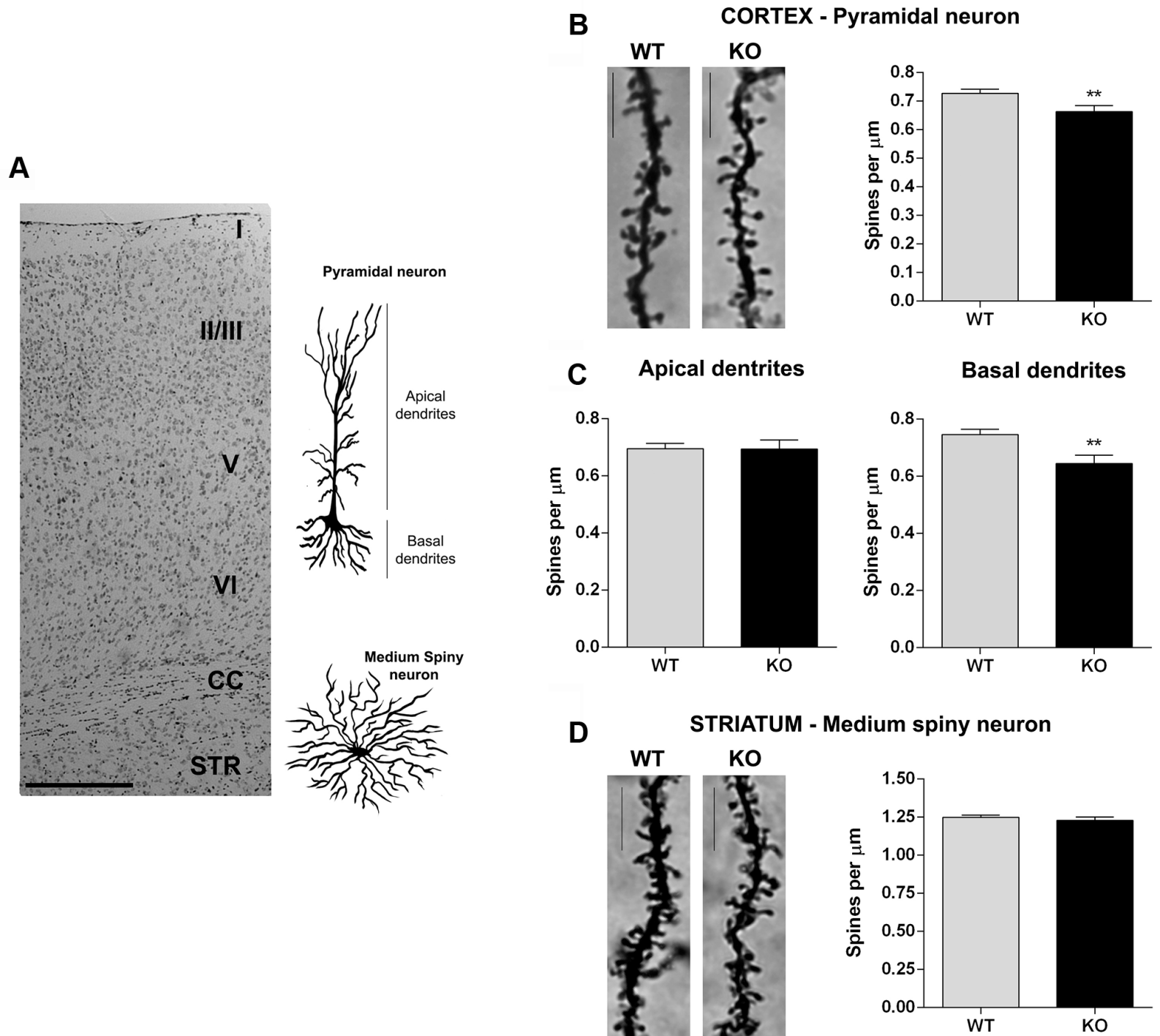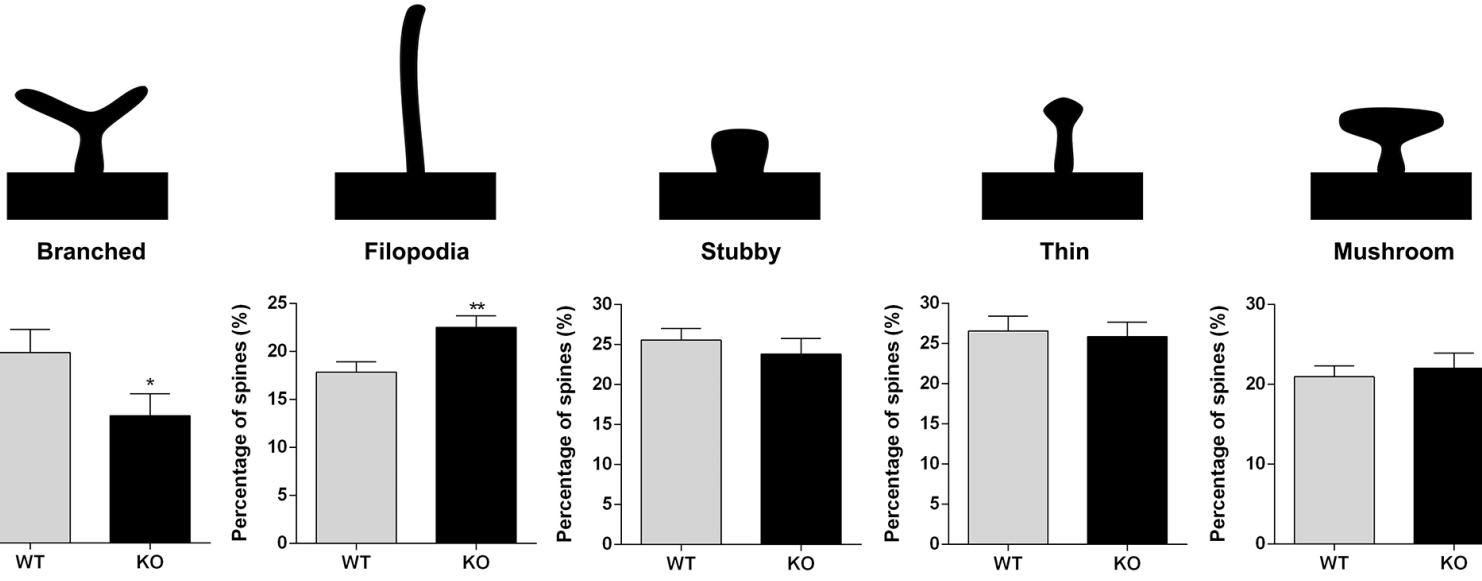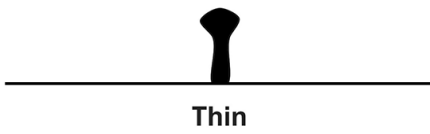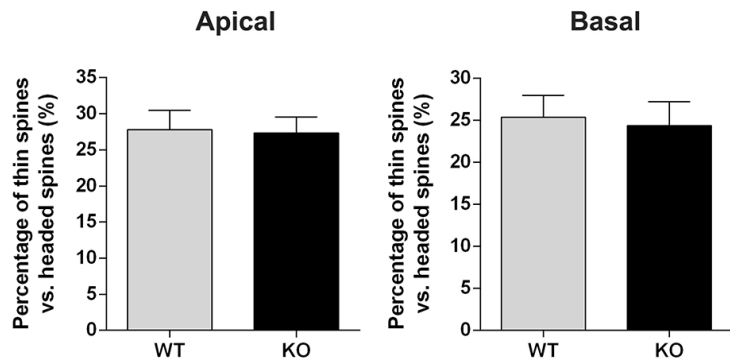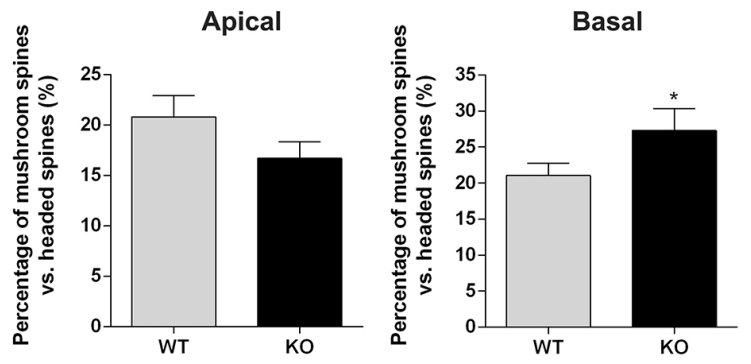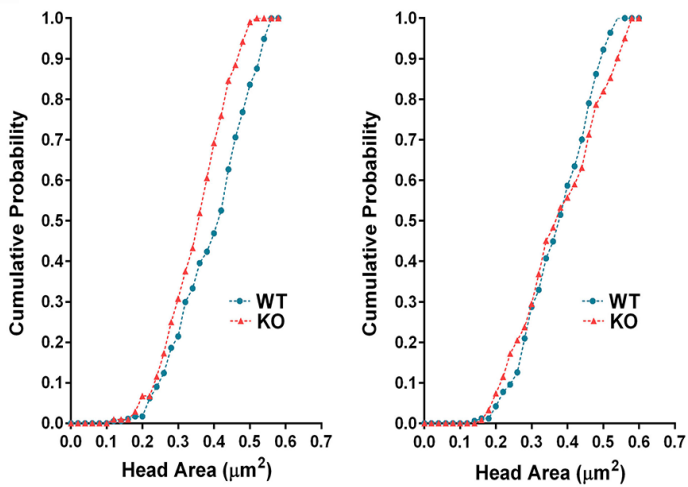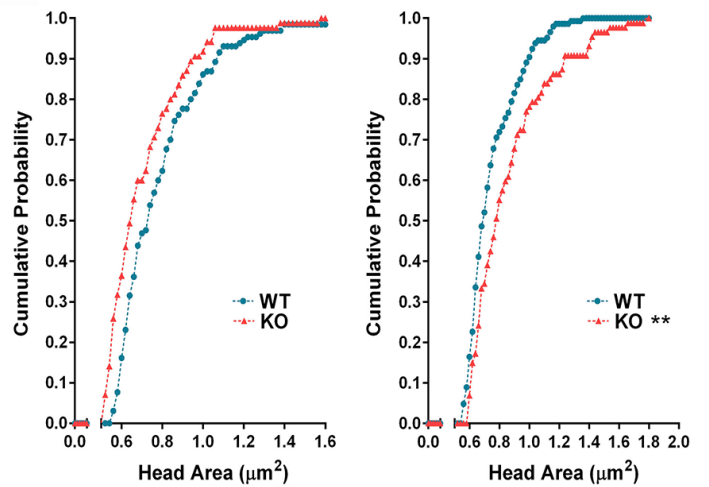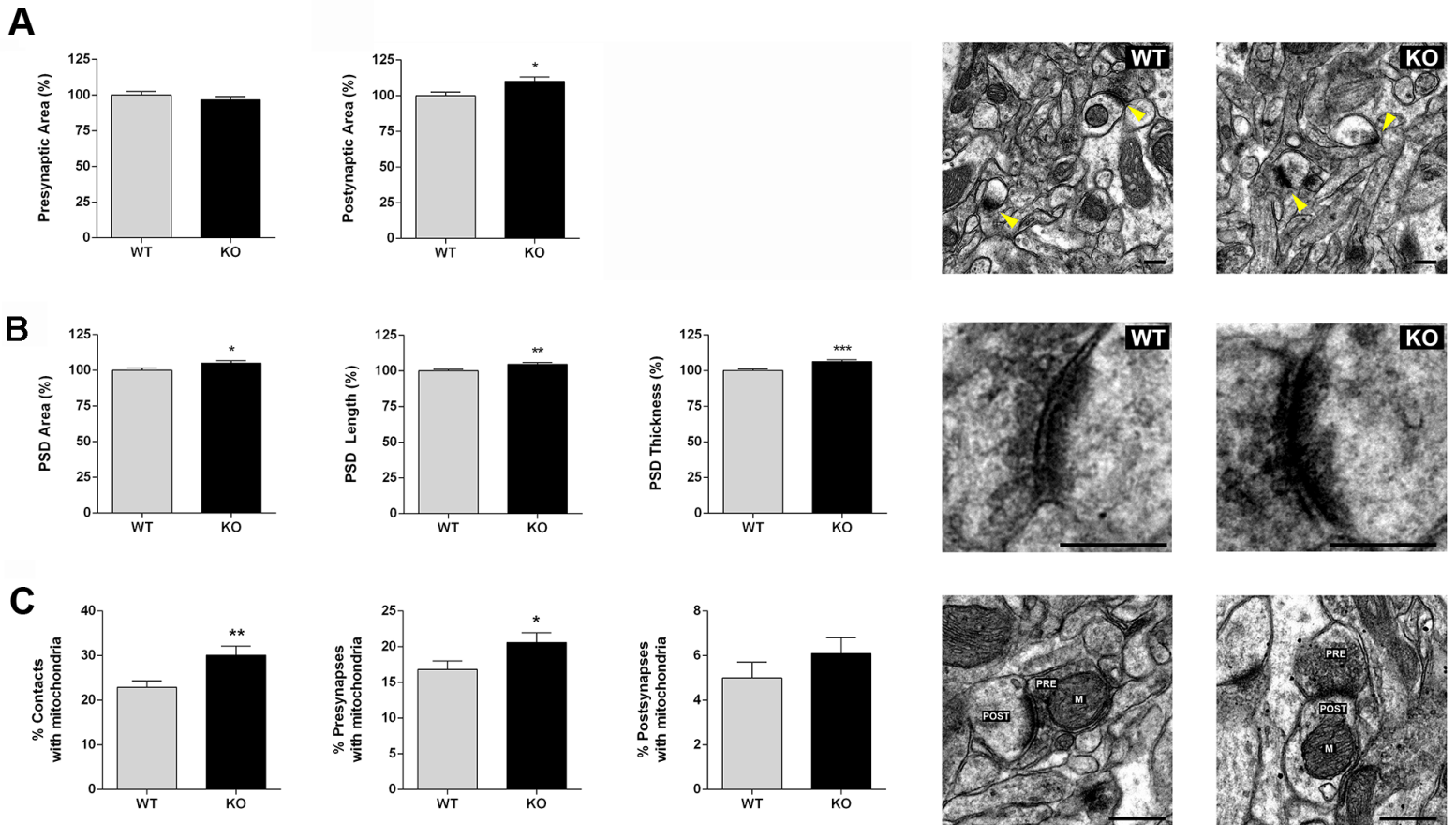
FIGURE 5

FIGURE 6

FIGURE 7
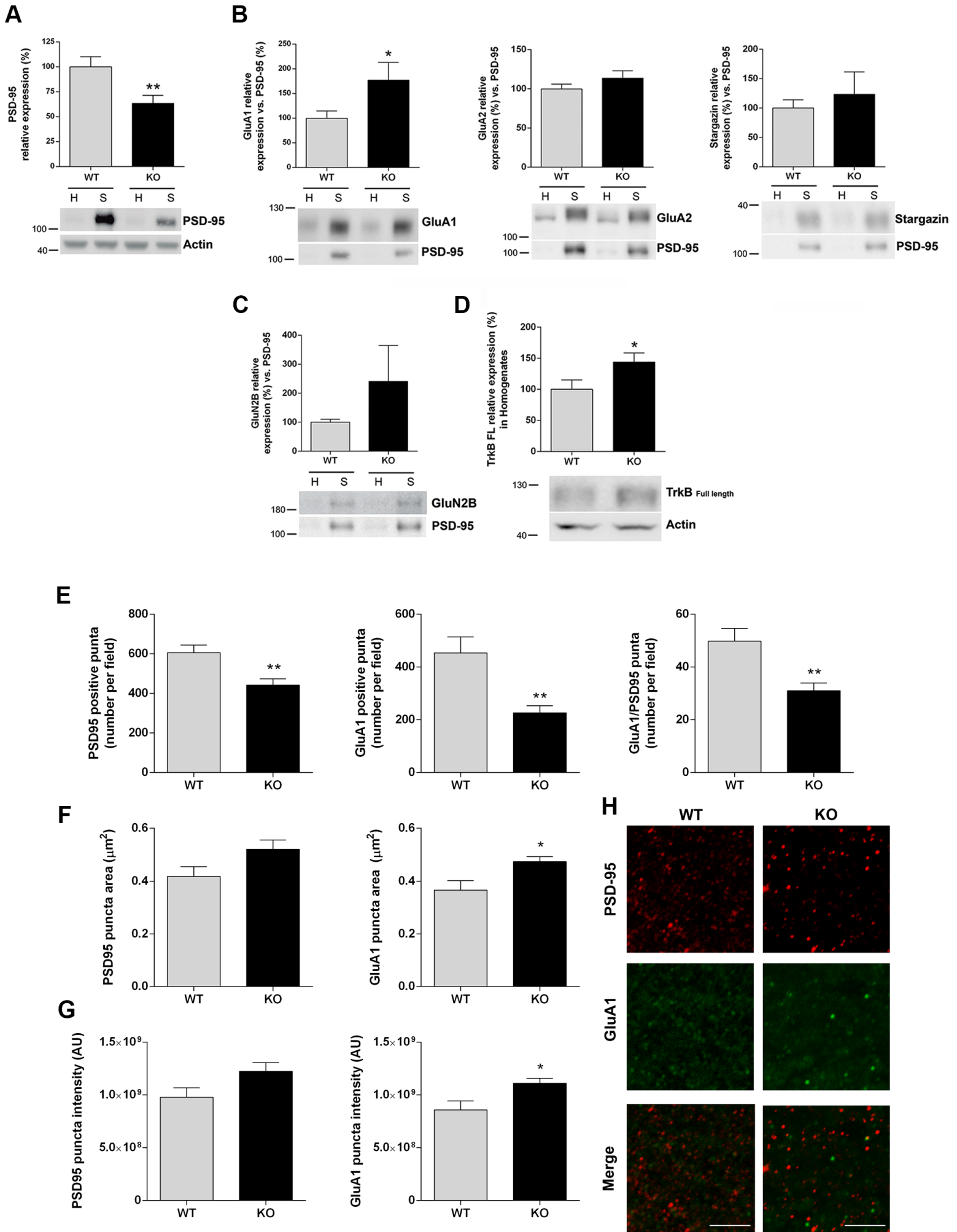
Motor CTX
LV pyramidal neuron

APICAL

BASAL

WT

KO
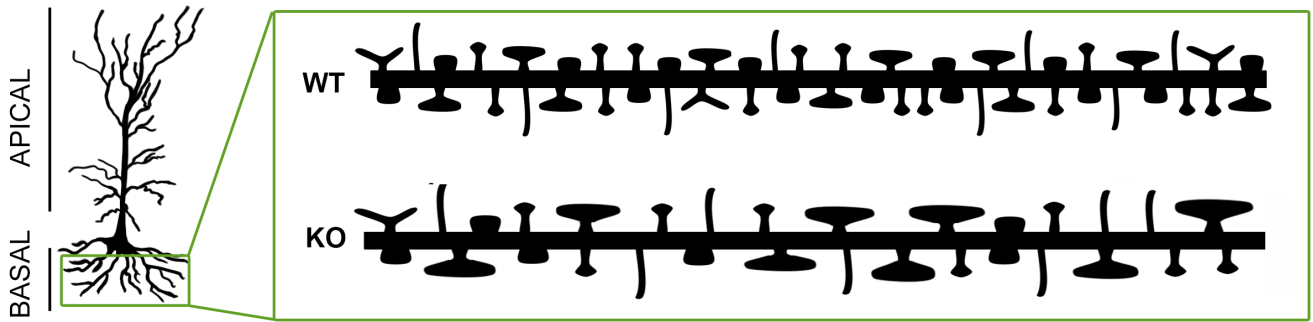
WT SYNAPSE

RTP801 KO SYNAPSE

RTP801

NMDA

TrkB

Mitochondria

Spine Apparatus

AMPAR (GluA2-containing, CI)
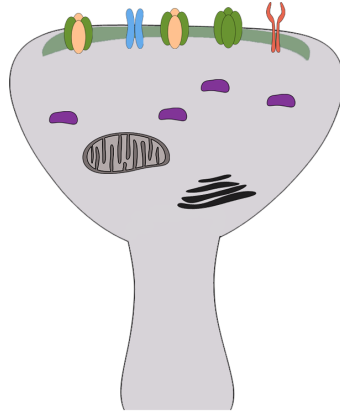
AMPAR (GluA1-containing, CP)
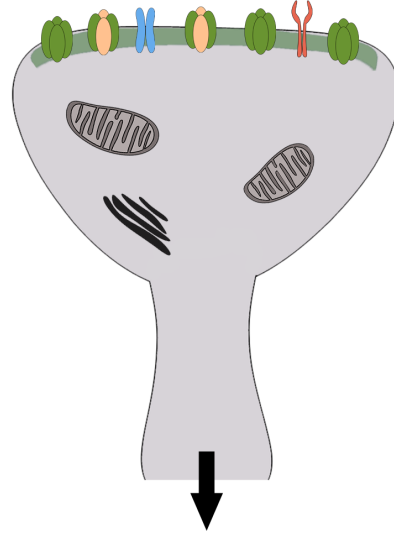
Improved motor learning skills
Increased amplitude and frequency of excitatory currents